Exolith Simulants Constituent Report

exolithlab@ucf.edu

July 2023

Table of Contents

1 Context

Our goal is to develop and produce high-fidelity mineralogical simulants for the Moon, Mars, and asteroids. While one could make a chemically similar simulant for well-characterized planetary regolith using laboratory grade oxides, such a simulant would poorly reproduce many important regolith properties, including geotechnical properties. Mineralogy is the primary driver of these properties so we aim to simulate mineralogy in the correct proportions. Inevitably, naturally-occurring terrestrial minerals have experienced weathering and will contain at least small amounts of undesired mineral phases (contaminants). To control the quality of Exolith feedstock and identify reliable mineral sources with minimal contaminant phases, we verify the composition of each simulant constituent regularly.

The combination of X-ray fluorescence (XRF) and X-ray diffraction (XRD) techniques constrains mineral composition and can be used to identify the presence of contaminant phases. XRF analysis reveals the chemical composition of a sample. XRD analysis reveals crystal lattice spacing characteristic of particular mineral phases. The XRF and XRD data were acquired at the University of Central Florida's Materials Characterization Facility (MCF), with an exception for the basalt data as described in that section. All samples studied at the MCF were prepared as powders. The XRF data were acquired with a PANalytical Epsilon 1 XRF and concentrations of each compound were determined using Omnian software. The Epsilon 1 XRF uses a 50-kV silver X-ray tube. XRD data were acquired using a PANalytical Empyrean XRD Diffractometer. The Empyrean uses a 1.8-kW copper X-ray tube and a vertical goniometer with theta, theta geometry. We used HighScore software connected to the International Centre for Diffraction Data Powder Diffraction File to aid in XRD interpretation.

In 2021, reflectance spectra were obtained by Takahiro Hiroi at the Keck/NASA Reflectance Experiment Laboratory (RELAB; **http://www.planetary.brown.edu/relab/**). Visible-to-near-infrared spectra were obtained using a UV-Vis-NIR bidirectional reflectance spectrometer with an incidence angle of 30° and emergence angle of 0°. Mid-infrared (thermal) spectra were obtained using a Thermo Nexus 870 FT-IR spectrometer.

2 Simulant Constituent Analysis

2.1 Anorthosite

- Description: Igneous rock rich in plagioclase feldspar
- Source: Hudson Resources, Inc. GreenSpar
- Idealized Formula: $CaAl_2Si_2O_8$ (anorthite); $NaAl_2Si_2O_8$ (albite)

Notes Major phase anorthite confirmed by XRD analysis (Figure 2, Table 1). Presence of small quantities of albite also confirmed by XRD. The Hudson Resources website[1] reports that the GreenSpar anorthosite product is 90% plagioclase feldspar. Our XRF findings (Table 2) are consistent with those reported by Hudson and with the XRD results.

Figure 1. Photo of Greenspar Anorthosite

2.1.1 X-Ray Diffraction Pattern

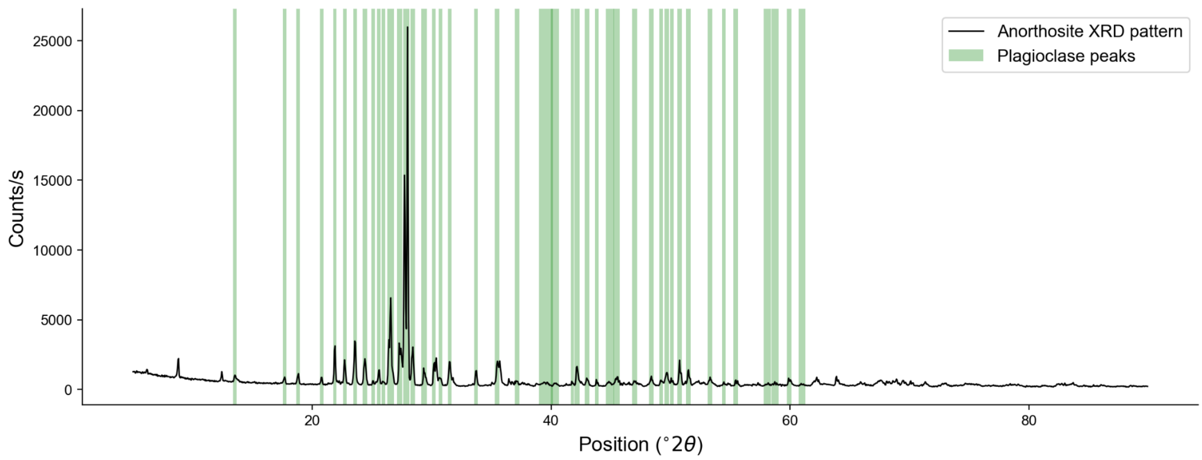

Figure 2: XRD pattern for anorthosite sample. [1]https://hudsonresourcesinc.com/

Table 1: Anorthosite - XRD Pattern Peaks

Position (°2θ)	*Relative Intensity (%)*	*d-spacing (Å)*	*Matched By*
5.89	5.3	15.00	
8.80	10.0	10.05	
12.44	4.9	7.11	
13.55	4.1	6.53	Anorthite, albite
17.70	3.2	5.01	Anorthite
18.83	4.3	4.71	Anorthite, albite
20.79	3.5	4.27	Anorthite
21.90	15.1	4.06	Anorthite, albite
22.73	9.7	3.91	Anorthite, albite
23.59	17.6	3.77	Anorthite, albite
24.42	10.2	3.65	Anorthite, albite
25.10	2.2	3.55	Anorthite
25.60	6.2	3.48	Anorthite, albite
25.96	1.7	3.43	Anorthite, albite
26.57	31.9	3.35	Anorthite, albite
27.33	14.5	3.26	Anorthite
27.73	73.3	3.22	Anorthite, albite
28.01	100.0	3.19	Anorthite, albite
28.42	14.0	3.14	Anorthite, albite
29.37	5.6	3.04	Anorthite
30.19	8.2	2.96	Anorthite, albite
30.74	3.0	2.91	Anorthite, albite
31.51	9.1	2.84	Anorthite, albite
33.73	5.8	2.66	Anorthite, albite
35.49	8.9	2.53	Anorthite, albite
37.16	1.9	2.42	Anorthite, albite
39.56	1.2	2.28	Albite
40.31	1.1	2.24	Albite
41.78	1.5	2.16	Albite
42.17	7.4	2.14	Albite
43.02	2.7	2.10	Albite
43.83	1.9	2.07	Albite
44.90	1.5	2.02	Albite
45.49	2.8	1.99	Albite
46.99	1.9	1.93	Albite
48.39	3.5	1.88	Albite
49.19	2.3	1.85	Albite
49.68	5.1	1.84	Albite
50.11	1.9	1.82	Albite
50.76	7.8	1.80	Albite
51.49	6.0	1.77	Albite
53.31	3.1	1.72	Albite
54.45	1.4	1.69	Albite
55.46	2.1	1.66	Albite
58.08	0.9	1.59	Albite
58.72	1.2	1.57	Albite
59.91	2.6	1.54	Albite
60.99	0.8	1.52	Albite
62.22	3.4	1.49	
63.86	3.7	1.46	
65.83	1.2	1.42	
67.62	2.2	1.39	
68.89	2.5	1.36	
69.42	2.1	1.35	
70.06	1.9	1.34	
71.30	1.6	1.32	
72.91	1.1	1.30	
74.87	1.0	1.27	
78.44	0.7	1.22	
82.37	0.8	1.17	
83.65	1.1	1.16	
85.96	0.3	1.13	

Peak match citation: PDF 98-002-2022 (anorthite), PDF 98-000-9830 (albite) in Gates-Rector and Blanton (2019)

2.1.2 Chemistry from X-Ray Fluorescence

Table 2: Anorthosite - Bulk Chemistry

Compound	*Concentration (wt%)*
Al_2O_3	29.4
SiO_2	49.3
P_2O_5	1.0
SO_3	0.1
Cl	0.1
K_2O	0.3
CaO	19.0
TiO_2	0.1
Fe_2O_3	0.7
Total	100.0

2.1.3 FTIR Spectroscopy

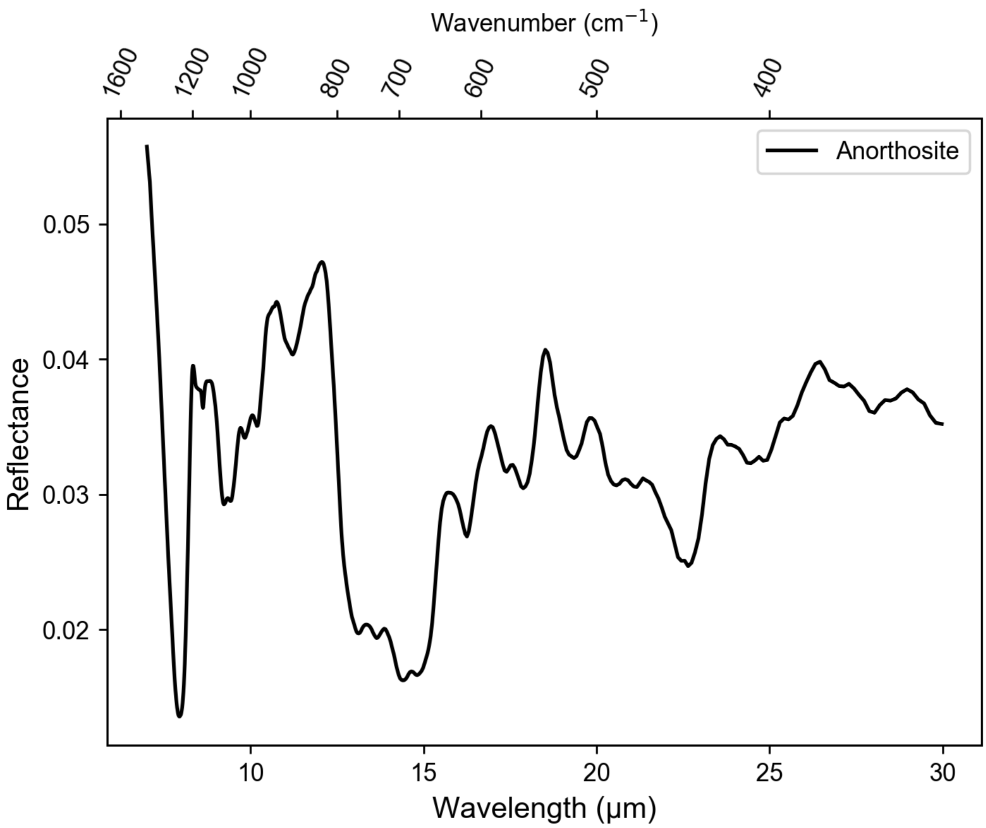

Figure 3. Anorthosite FTIR Spectroscopy

2.1.4 VIS NIR Spectroscopy

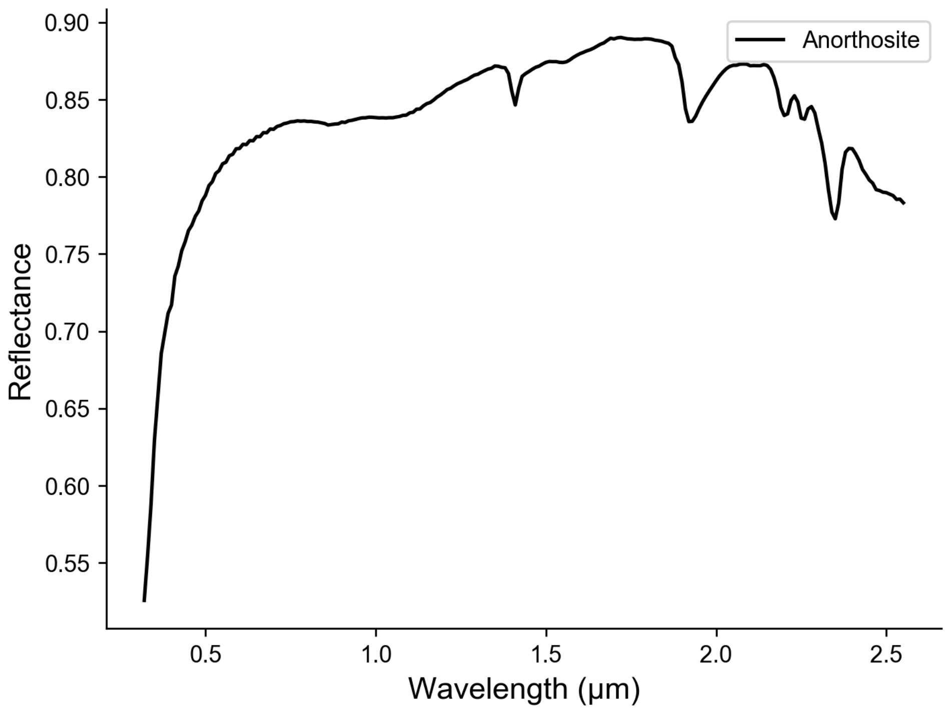

Figure 4. Anorthosite VIS NIR Spectroscopy

2.1.5 Particle Size Analysis

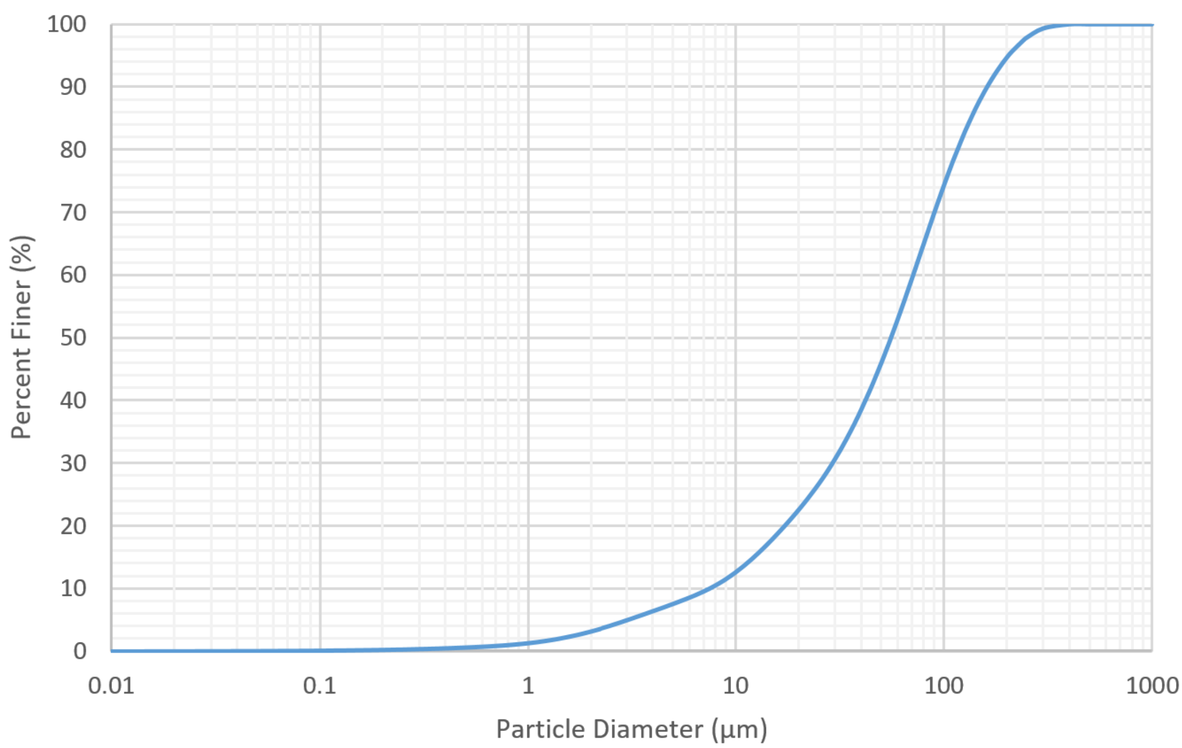

Figure 5. Anorthosite Particle Size Distribution

2.2 Attapulgite

- Description: Phyllosilicate
- Source: MIN-U-GEL
- Idealized Formula: $(Mg,Al)_2Si_4O_{10}(OH)\cdot 4(H_2O)$
- Also called: Palygorskite

Notes Major phase confirmed by XRD analysis (Figure 7, Table 3). XRF analysis (Table 4) is consistent with a main phase of a magnesium aluminum silicate. XRF also indicates presence of calcium (9.2 wt% CaO) and iron (6.7 wt% Fe_2O_3), perhaps indicating a contaminant phase.

Figure 6: Photo of Attapulgite.

2.2.1 X-Ray Diffraction Pattern

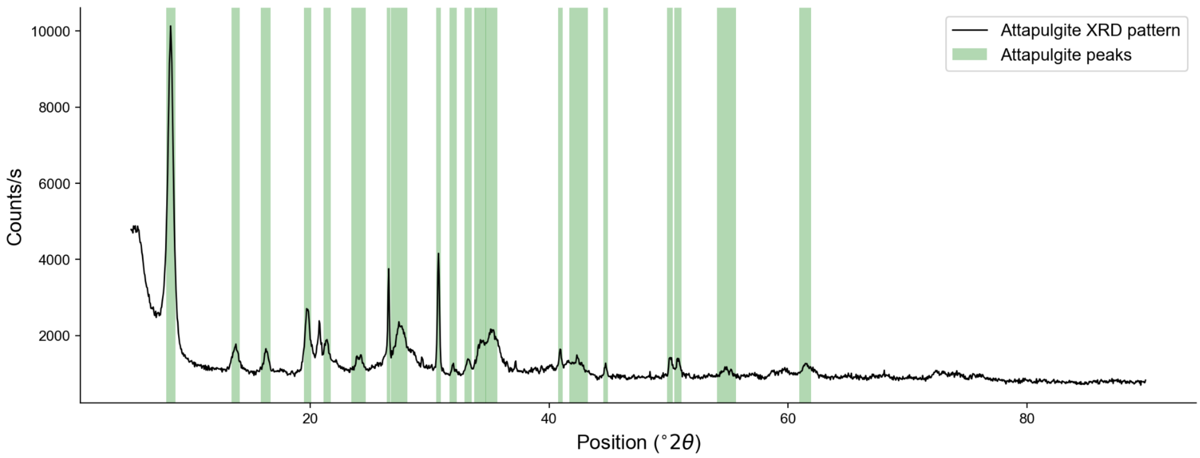

Figure 7: XRD pattern for Attapulgite sample. Diagnostic peaks are labeled with corresponding d spacing.

Table 3: Attapulgite - XRD Pattern Peaks

Position (°2θ)	*Relative Intensity (%)*	*d-spacing (Å)*	*Matched By*
5.74	40.3	15.41	
8.34	100.0	10.60	Attapulgite
13.76	9.2	6.44	Attapulgite
16.29	7.7	5.44	Attapulgite
19.80	19.5	4.48	Attapulgite
20.78	16.1	4.28	
21.43	10.8	4.15	Attapulgite
24.06	5.5	3.70	Attapulgite
26.57	30.2	3.35	Attapulgite
27.45	15.2	3.25	Attapulgite
30.74	34.0	2.91	Attapulgite
31.98	3.4	2.80	Attapulgite
33.23	5.2	2.70	Attapulgite
34.23	9.8	2.62	Attapulgite
35.20	13.5	2.55	Attapulgite
40.93	8.1	2.21	Attapulgite
42.47	5.0	2.13	Attapulgite
44.72	3.9	2.03	Attapulgite
50.10	5.6	1.82	Attapulgite
50.78	5.0	1.80	Attapulgite
54.83	2.5	1.67	Attapulgite
61.43	3.8	1.51	Attapulgite
72.30	1.7	1.31	

Peak match citation: PDF 98-004-0687 in Gates-Rector and Blanton (2019)

2.2.2 Chemistry from X-Ray Fluorescence

Table 4. Attapulgite - Bulk Chemistry

Compound	*Concentration (wt%)*
MgO	11.5
Al_2O_3	10.8
SiO_2	57.2
P_2O_5	2.0
SO_3	0.1
Cl	0.2
K_2O	1.1
CaO	9.2
TiO_2	1.0
Cr_2O_3	<0.1
MnO	0.1
Fe_2O_3	6.7
Total	99.9

2.2.3 FTIR Spectroscopy

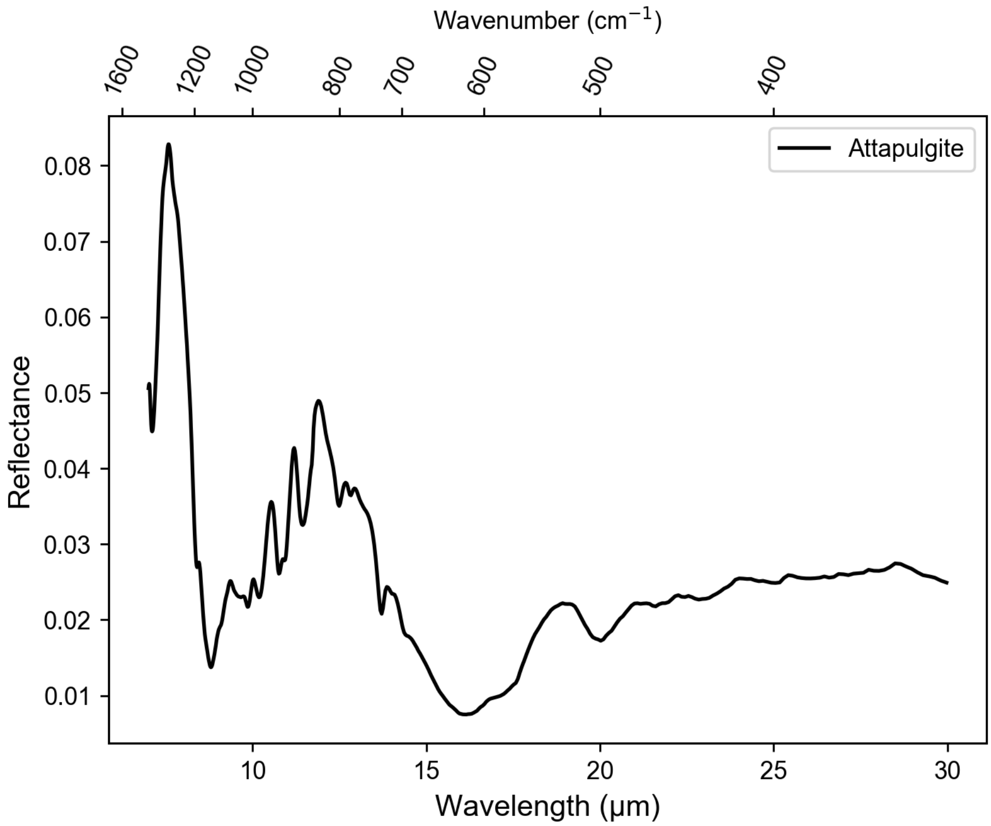

Figure 8. Attapulgite FTIR Spectroscopy

2.2.4 VIS NIR Spectroscopy

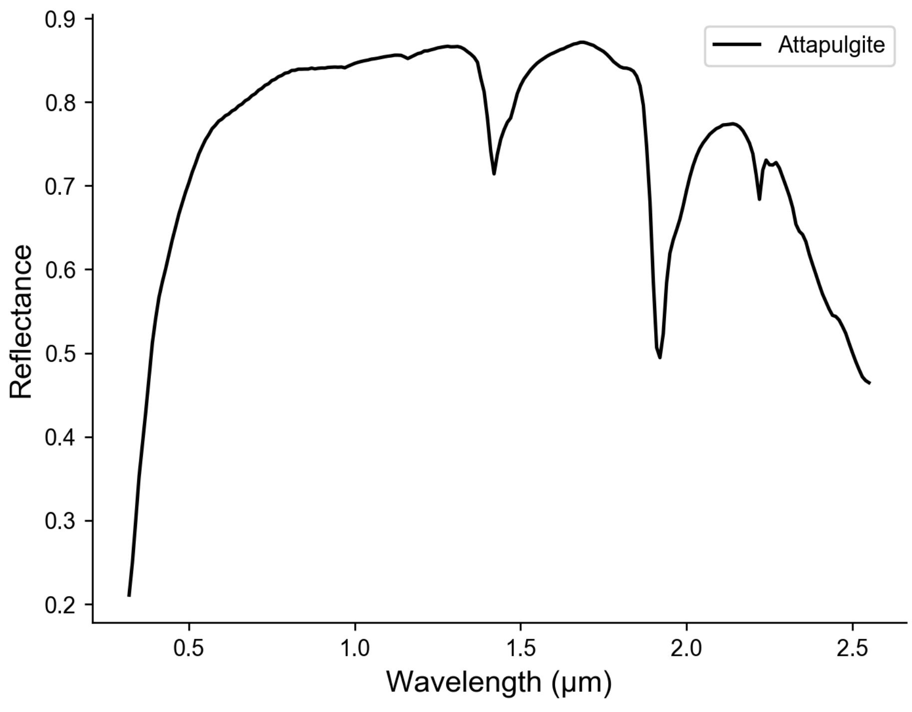

Figure 9. Attapulgite VIS NIR Spectroscopy

2.2.5 Particle Size Analysis

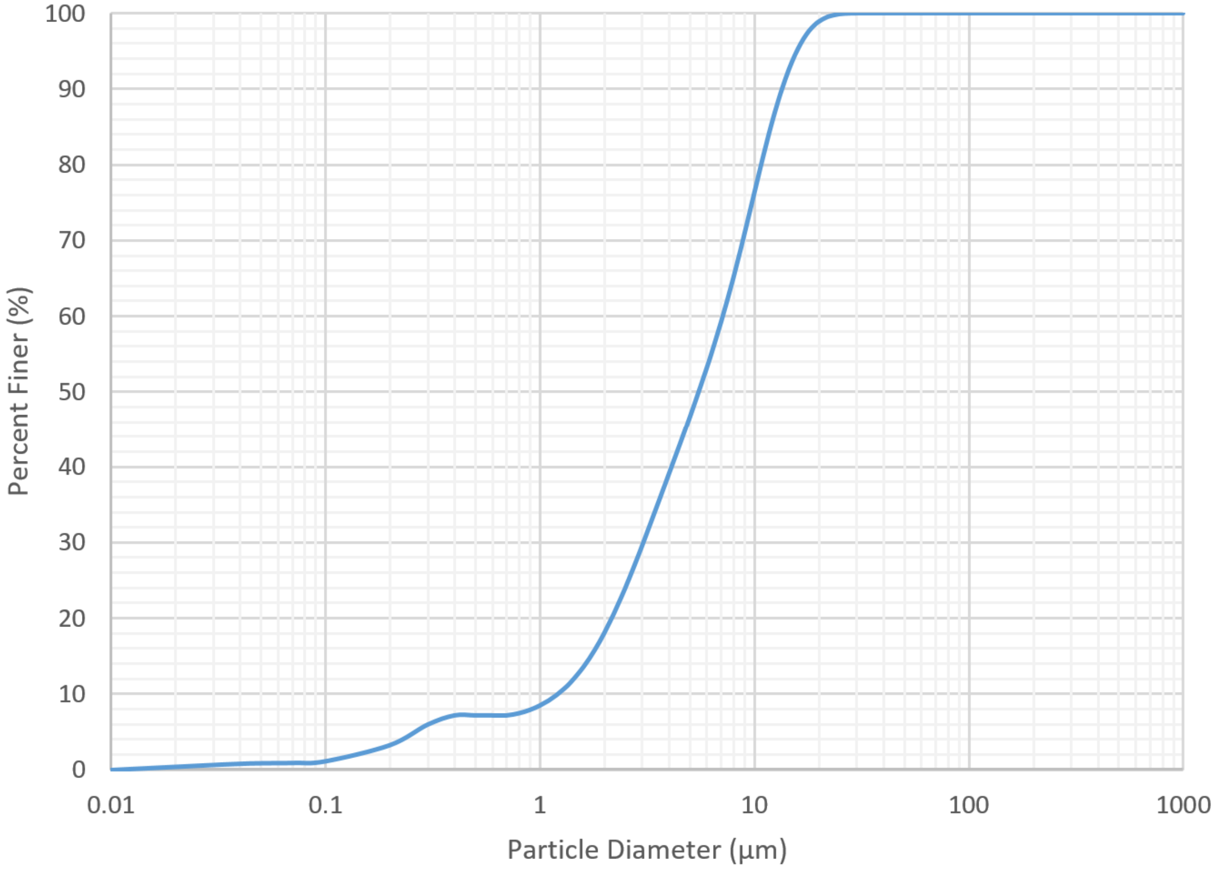

Figure 10. Attapulgite Particle Size Distribution

2.3 Basalt (Glass-Rich)

• Description: Mafic igneous rock containing plagioclase, pyroxene, olivine, and volcanic glass •

Source: Merriam Crater Basalt sourced from the Merriam Crater near Flagstaff, AZ.

This is the same source as JSC-1A

Figure 11: Photo of Basalt.

2.3.1 Chemistry from X-Ray Fluorescence

Table 5: Basalt (Glass-Rich) - Approximate Bulk Chemistry

Compound	Concentration (wt %)
SiO_2	47.71
TiO_2	1.59
Al_2O_3	15.02
Fe_2O_3	10.79
MnO	0.19
MgO	9.39
CaO	9.9
Na_2O	2.7
K_2O	0.82
P_2O_5	0.66
Total	98.77

2.3.2 Particle Size Analysis

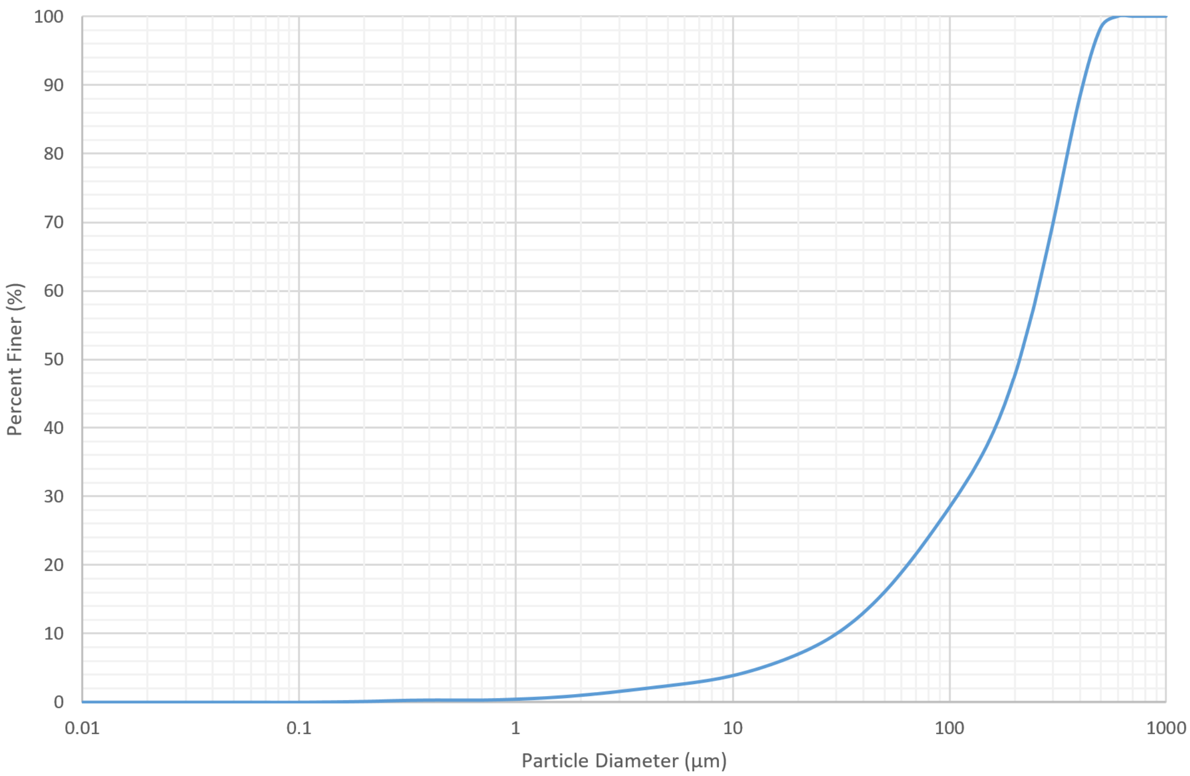

Figure 12. Basalt Particle Size Distribution

2.4 Bronzite

- Description: Pyroxene-group mineral
- Source: Stillwater Mine
- Idealized Formula: $(Mg,Fe)_3SiO_3$

Notes Major phase confirmed by XRD analysis (Figure 14, Table 6). The XRF results (Table 7) are consistent with the expected composition of bronzite.

Figure 13: Photo of bronzite.

2.4.1 X-Ray Diffraction Pattern

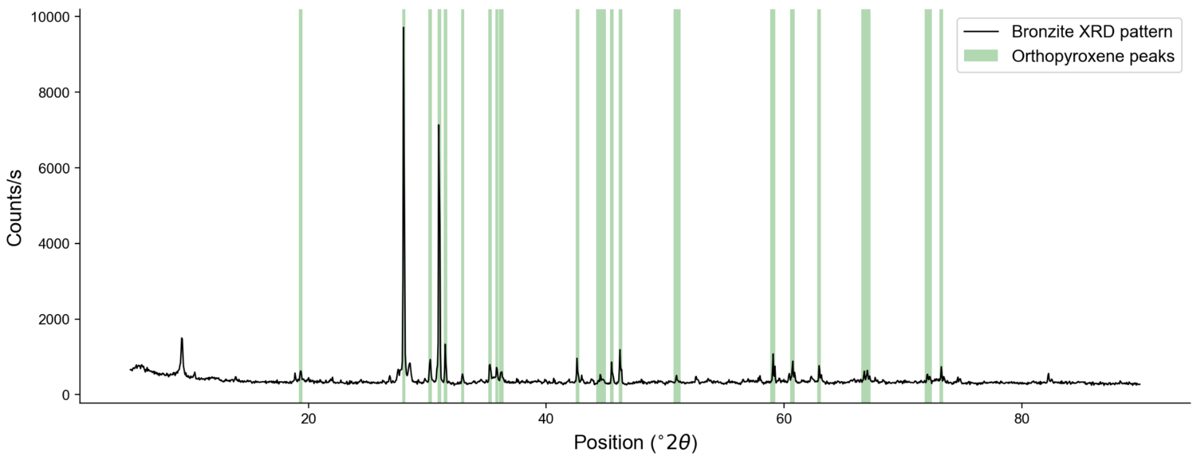

Figure 14: XRD Pattern for Bronzite Sample.

Table 6: Bronzite - XRD Pattern Peaks

Position (°2θ)	*Relative Intensity (%)*	*d-spacing (Å)*	*Matched By*
5.77	5.0	15.31	
9.37	15.2	9.44	
19.35	4.1	4.59	Orthopyroxene ($Mg_{2.83}Fe_{1.17}$)Si_4O_{12})
28.02	100.0	3.18	Orthopyroxene ($Mg_{2.83}Fe_{1.17}$)Si_4O_{12})
28.52	7.2	3.13	
30.23	8.0	2.96	Orthopyroxene ($Mg_{2.83}Fe_{1.17}$)Si_4O_{12})
30.99	80.2	2.89	Orthopyroxene ($Mg_{2.83}Fe_{1.17}$)Si_4O_{12})
31.52	10.5	2.84	Orthopyroxene ($Mg_{2.83}Fe_{1.17}$)Si_4O_{12})
32.97	2.8	2.72	Orthopyroxene ($Mg_{2.83}Fe_{1.17}$)Si_4O_{12})
35.27	6.3	2.54	Orthopyroxene ($Mg_{2.83}Fe_{1.17}$)Si_4O_{12})
35.85	5.3	2.50	Orthopyroxene ($Mg_{2.83}Fe_{1.17}$)Si_4O_{12})
36.22	3.9	2.48	Orthopyroxene ($Mg_{2.83}Fe_{1.17}$)Si_4O_{12})
42.62	5.4	2.12	Orthopyroxene ($Mg_{2.83}Fe_{1.17}$)Si_4O_{12})
44.61	1.8	2.03	Orthopyroxene ($Mg_{2.83}Fe_{1.17}$)Si_4O_{12})
45.53	4.6	1.99	Orthopyroxene ($Mg_{2.83}Fe_{1.17}$)Si_4O_{12})
46.22	7.9	1.96	Orthopyroxene ($Mg_{2.83}Fe_{1.17}$)Si_4O_{12})
51.00	1.4	1.79	Orthopyroxene ($Mg_{2.83}Fe_{1.17}$)Si_4O_{12})
59.04	7.0	1.56	Orthopyroxene ($Mg_{2.83}Fe_{1.17}$)Si_4O_{12})
60.69	6.3	1.53	Orthopyroxene ($Mg_{2.83}Fe_{1.17}$)Si_4O_{12})
62.95	6.1	1.48	Orthopyroxene ($Mg_{2.83}Fe_{1.17}$)Si_4O_{12})
66.87	2.2	1.40	Orthopyroxene ($Mg_{2.83}Fe_{1.17}$)Si_4O_{12})
72.13	2.1	1.31	Orthopyroxene ($Mg_{2.83}Fe_{1.17}$)Si_4O_{12})
73.21	4.9	1.29	Orthopyroxene ($Mg_{2.83}Fe_{1.17}$)Si_4O_{12})
74.70	1.3	1.27	
82.22	3.6	1.17	

Peak match citation: PDF 98-018-8072 in Gates-Rector and Blanton (2019)

2.4.2 Chemistry from X-Ray Fluorescence

Table 7: Bronzite - Bulk Chemistry

Compound	*Concentration (wt%)*
MgO	27.5
Al_2O_3	3.3
SiO_2	45.0
P_2O_5	1.1
SO_3	0.1
Cl	0.2
K_2O	0.1
CaO	4.8
TiO_2	0.3
Cr_2O_3	0.7
MnO	0.3
Fe_2O_3	16.5
NiO	0.1
Total	99.9

2.4.3 FTIR Spectroscopy

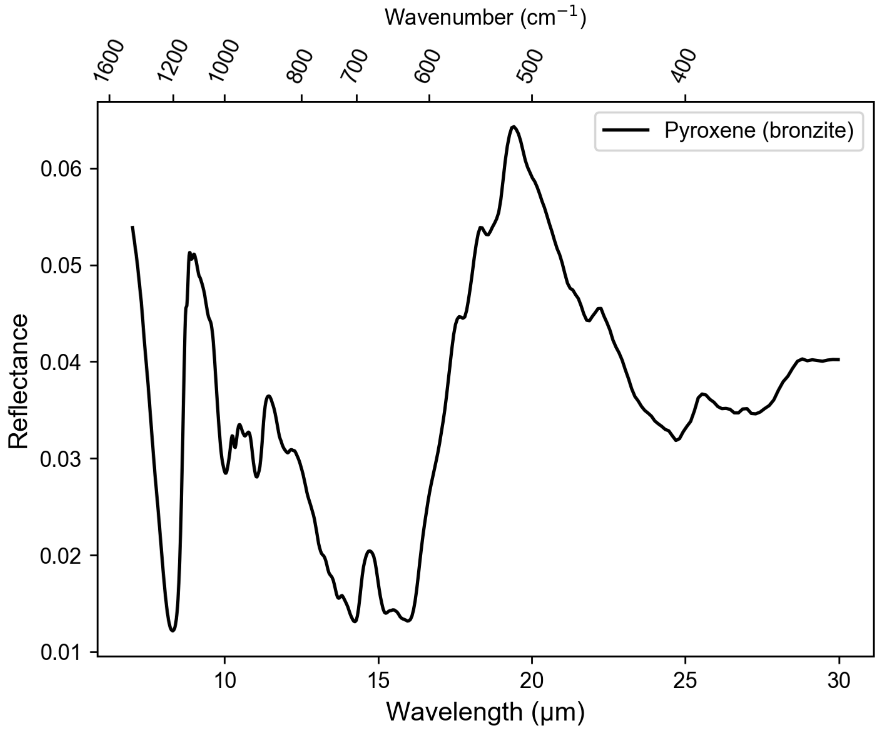

Figure 15: Bronzite FTIR Spectroscopy

2.4.4 VIS NIR Spectroscopy

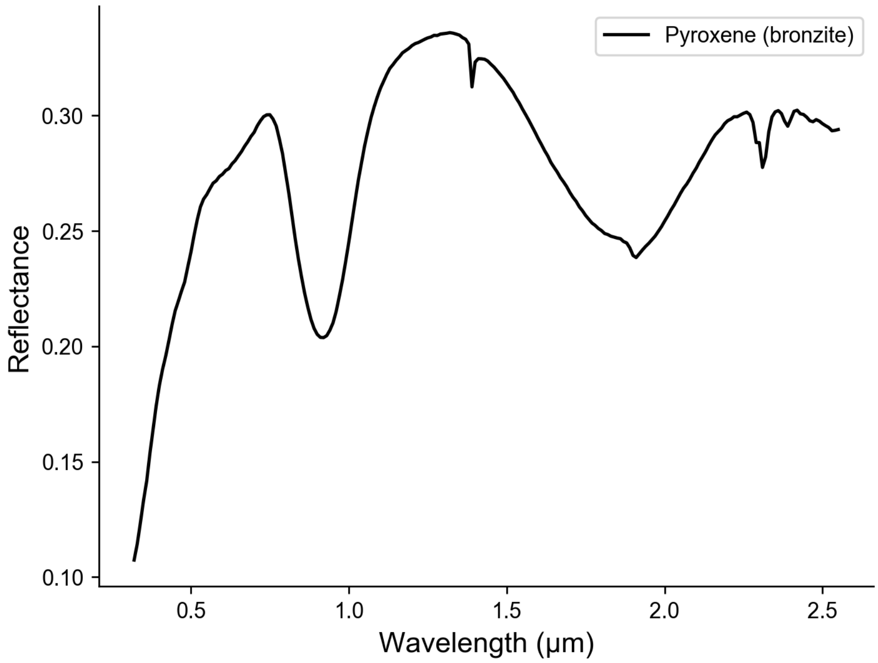

Figure 16: Bronzite VIS NIR Spectroscopy

2.4.5 Particle Size Analysis

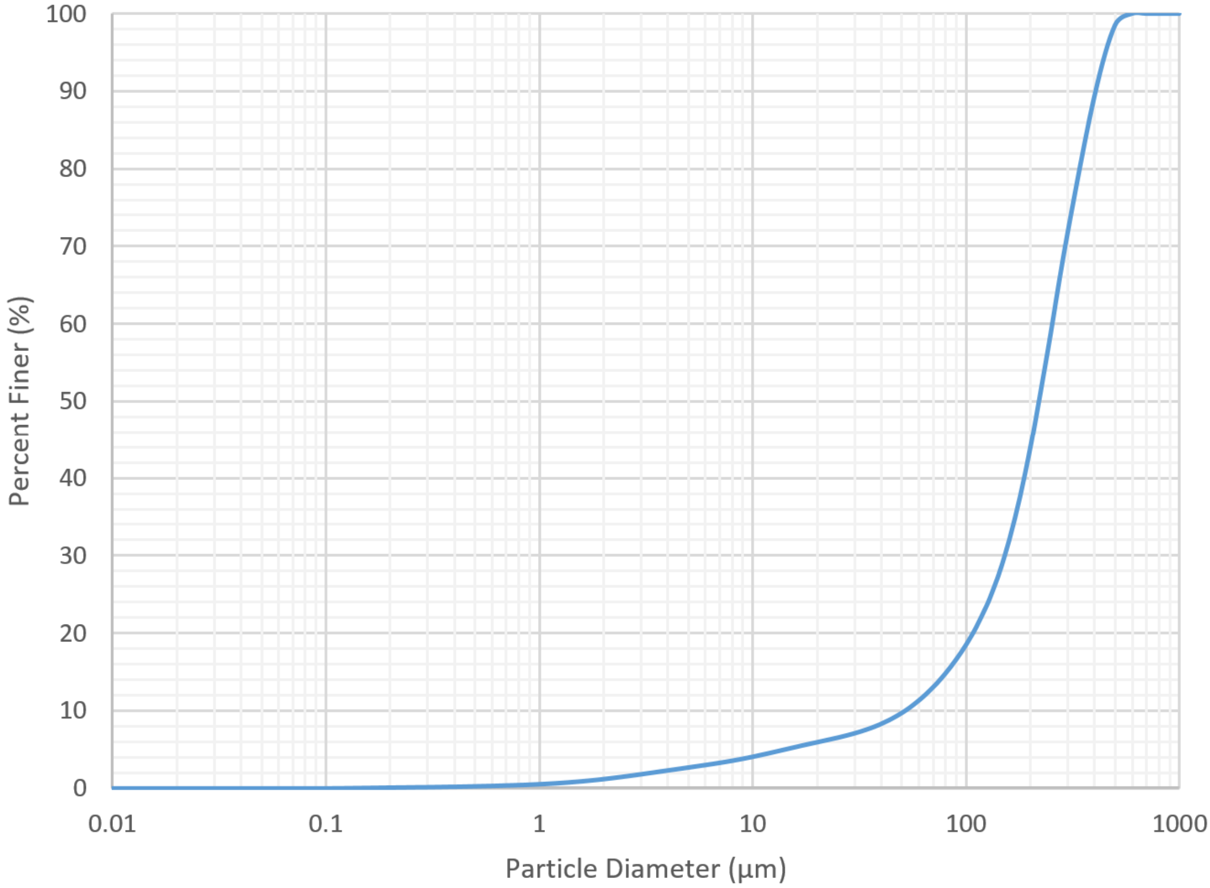

Figure 17. Bronzite Particle Size Distribution

2.5 Ferrihydrite

- Description: Hydrous ferric oxyhydroxide mineral
- Source: Kolar Labs High Capacity Granular Ferric Oxide (HC GFO)
- Idealized Formula: $(Fe^{3+})_2O_3 \cdot 0.5H_2O$

Notes: XRD analysis (Figure 19, Table 8) confirms the primary phase is two-line ferrihydrite (2LFh), so named for its two XRD peaks (Vaughan et al., 2012); the more structured form of ferrihydrite shows 6 XRD peaks (Figure 20). Only the strongest of the two peaks, at 2θ = 35.8122°, was identified by algorithm, although the expected secondary peak at 2θ = 63.50° is identifiable by eye. XRF analysis (Table 9). confirms > 92% Fe_2O_3.

Figure 18: Photo of Ferrihydrite.

2.5.1 X-Ray Diffraction Pattern

Table 8: Ferrihydrite - XRD Pattern Peaks

Position (°2θ)	*Relative Intensity (%)*	*d-spacing (Å)*	*Matched By*
35.8122	100	2.50538	Two-line ferrihydrite
63.50	– (ID’d by eye)	– (ID’d by eye)	Two-line ferrihydrite

Peak match citation: Vaughan et al. (2012)

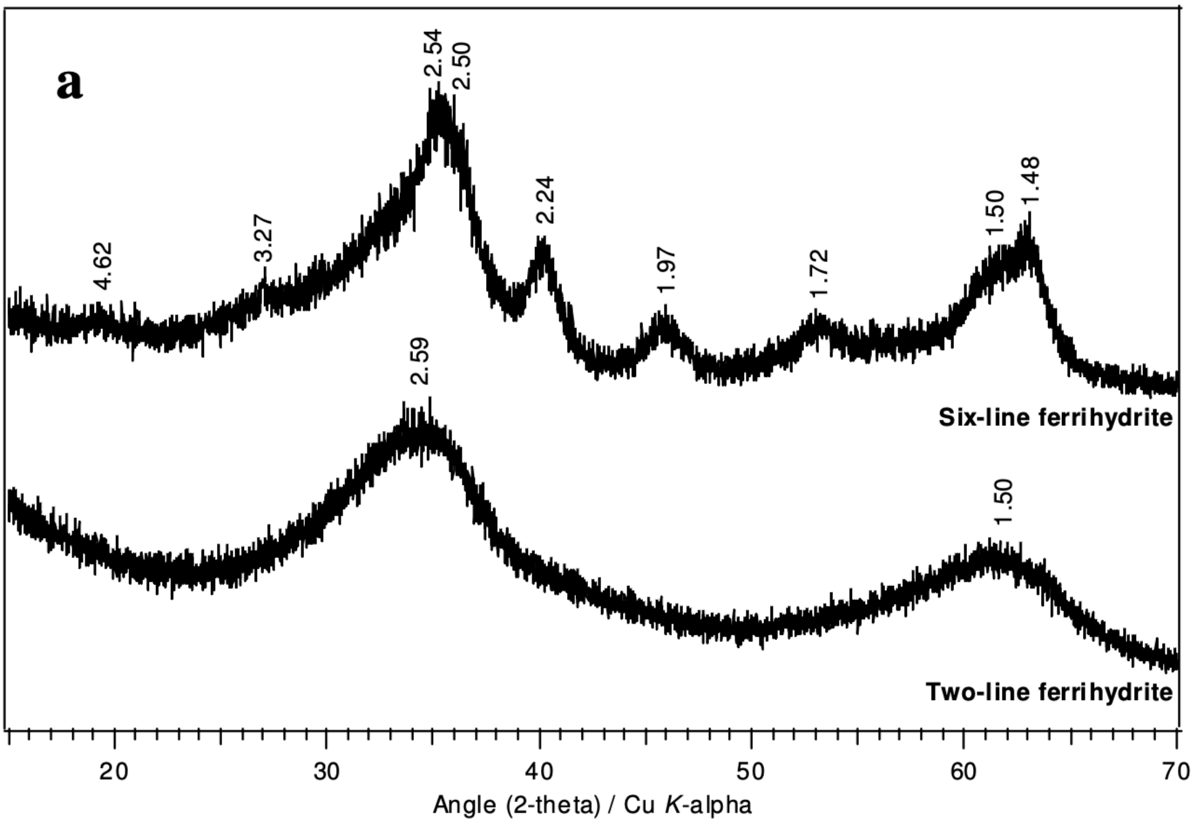

Figure 19: From Vaughan et al. (2012): powder XRD patterns for both two- and six-line ferrihydrite.

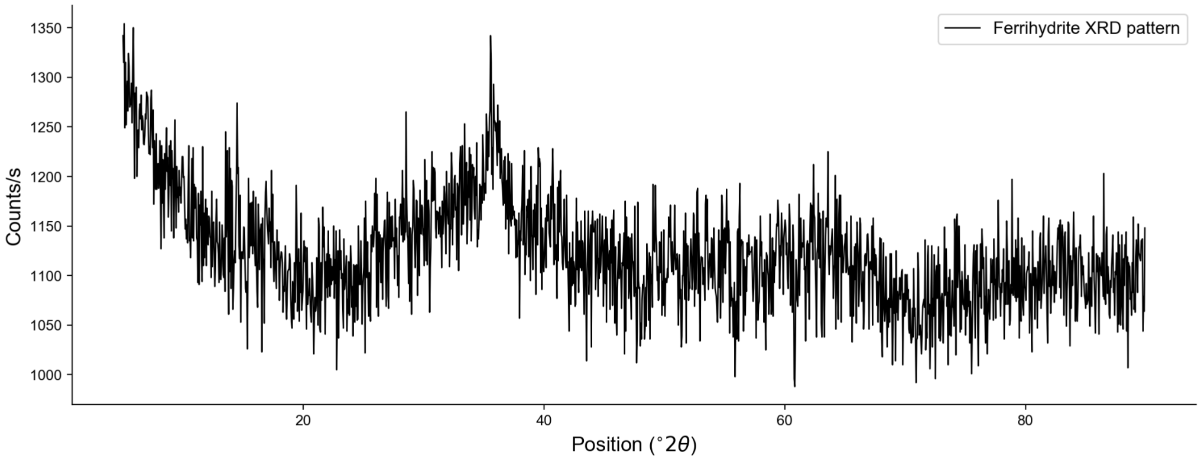

Figure 20: XRD pattern for ferrihydrite sample.

2.5.2 Chemistry from X-Ray Fluorescence

Table 9: Ferrihydrite - Bulk Chemistry

Compound	*Concentration (wt%)*
MgO	5.3
Al_2O_3	0.3
P_2O_5	0.7
SO_3	0.2
Cl	0.1
CaO	0.3
Cr_2O_3	0.1
MnO	0.2
Fe_2O_3	92.6
NiO	0.1
Rb_2O	0.0
HfO_2	<0.1
Total	99.9

2.5.3 FTIR Spectroscopy

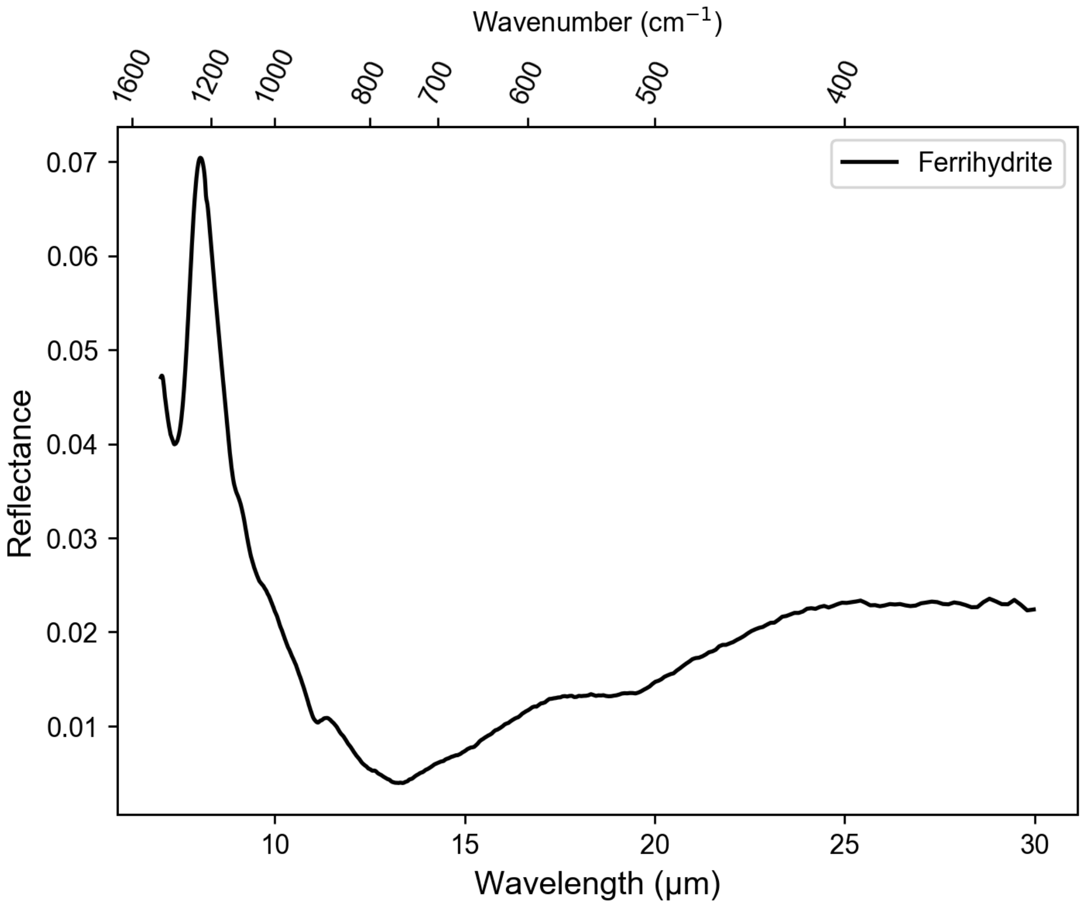

Figure 21: Ferrihydrite FTIR Spectroscopy

2.5.4 VIS NIR Spectroscopy

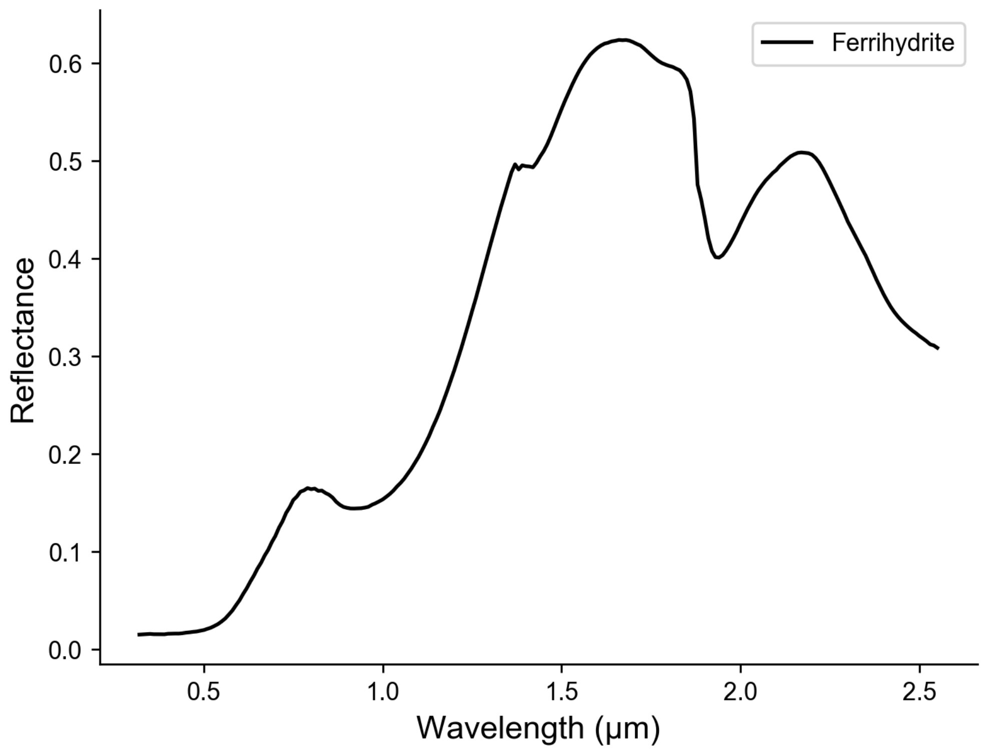

Figure 22: Ferrihydrite FTIR Spectroscopy

2.5.5 Particle Size Analysis

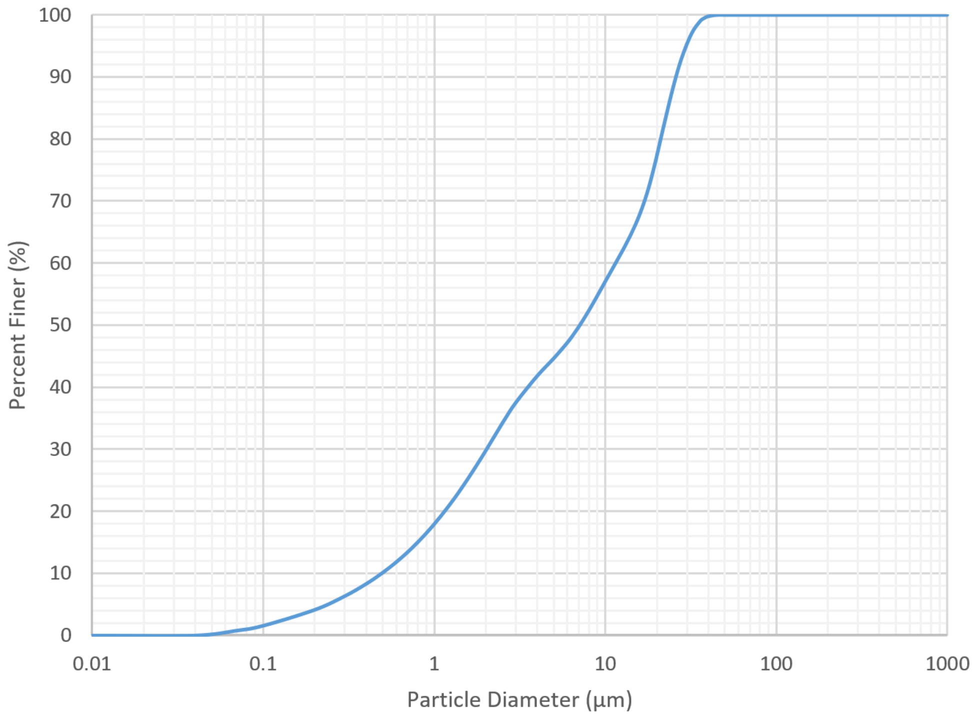

Figure 23. Ferrihydrite Particle Size Distribution

2.6 Gypsum

- Description: Calcium sulfate
- Source: –
- Idealized Formula: $CaSO_4 \cdot 2H_2O$

Notes Major phase confirmed by XRD analysis (Figure 25, Table 10). Additional peaks indicate the presence of a minor contaminant phase. XRF analysis (Table 11) confirms CaO and SO_3 are the major compounds present.

Figure 24: Photo of Gypsum.

2.6.1 X-Ray Diffraction Pattern

Table 10: Gypsum- XRD Pattern Peaks

Position (°2θ)	*Relative Intensity (%)*	*d-spacing (Å)*	*Matched By*
6.18	1.0	14.29	
8.72	13.9	10.14	
9.42	1.4	9.38	
10.46	1.2	8.46	
11.59	100.0	7.63	Gypsum
12.43	1.1	7.12	
17.52	0.5	5.06	
18.70	0.7	4.75	
20.69	8.6	4.29	Gypsum
23.36	11.8	3.81	Gypsum
24.06	0.1	3.70	
25.07	0.8	3.55	
26.43	5.1	3.37	
27.94	0.6	3.19	
28.55	0.7	3.13	
29.09	8.2	3.07	Gypsum
29.42	0.3	3.04	
30.93	3.8	2.89	Gypsum
31.50	0.2	2.84	
32.03	0.2	2.79	Gypsum
33.34	1.0	2.69	Gypsum
34.50	0.5	2.60	Gypsum
35.44	0.5	2.53	Gypsum
35.95	0.2	2.50	Gypsum
36.60	0.7	2.46	Gypsum
37.38	0.2	2.41	Gypsum
39.48	0.1	2.28	Gypsum
40.62	0.7	2.22	Gypsum
42.15	0.1	2.14	Gypsum
43.33	0.6	2.09	Gypsum
43.62	0.3	2.07	Gypsum
44.18	0.3	2.05	Gypsum
44.82	0.6	2.02	
45.49	0.4	1.99	Gypsum
47.82	1.2	1.90	Gypsum
48.36	0.4	1.88	Gypsum
48.72	0.2	1.87	Gypsum
50.30	0.7	1.81	Gypsum
51.32	0.5	1.78	Gypsum
53.58	0.1	1.71	Gypsum
54.43	0.1	1.69	Gypsum
55.10	0.3	1.67	Gypsum
56.70	0.8	1.62	Gypsum
58.10	0.2	1.59	Gypsum
60.34	0.1	1.53	Gypsum
63.67	0.2	1.46	Gypsum
64.57	0.1	1.44	Gypsum
65.86	0.1	1.42	Gypsum
67.33	0.2	1.39	
68.62	0.5	1.37	Gypsum
70.60	0.3	1.33	Gypsum
71.15	0.2	1.33	Gypsum
74.04	0.1	1.28	Gypsum
74.93	0.1	1.27	Gypsum
76.45	0.2	1.25	Gypsum
76.93	0.1	1.24	
79.58	0.1	1.20	
83.25	0.2	1.16	
84.94	0.1	1.14	
85.90	0.1	1.13	

Peak match citation: PDF 00-033-0311 in Gates-Rector and Blanton (2019)

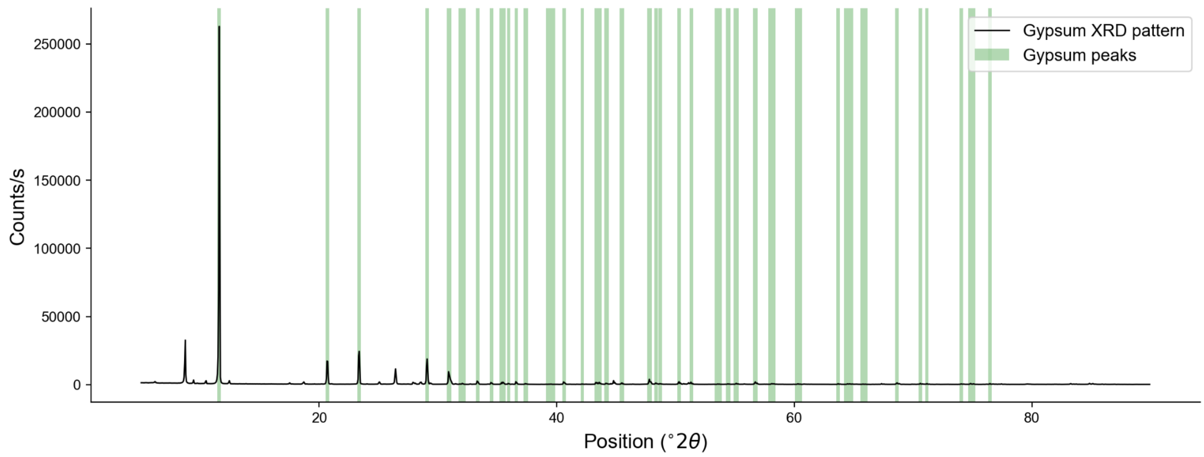

Figure 25: XRD pattern for gypsum sample shown with a reference pattern (Schofield et al., 1996). 2.6.2 Chemistry from X-Ray Fluorescence

2.6.2 Chemistry from X-Ray Fluorescence

Table 11: Gypsum - Bulk Chemistry

Compound	*Concentration (wt%)*
MgO	4.8
Al_2O_3	1.9
SiO_2	4.2
P_2O_5	0.7
SO_3	45.0
Cl	0.1
K_2O	0.5
CaO	41.9
TiO_2	0.2
Fe_2O_3	0.5
SrO	0.2
Total	100.0

2.6.3 FTIR Spectroscopy

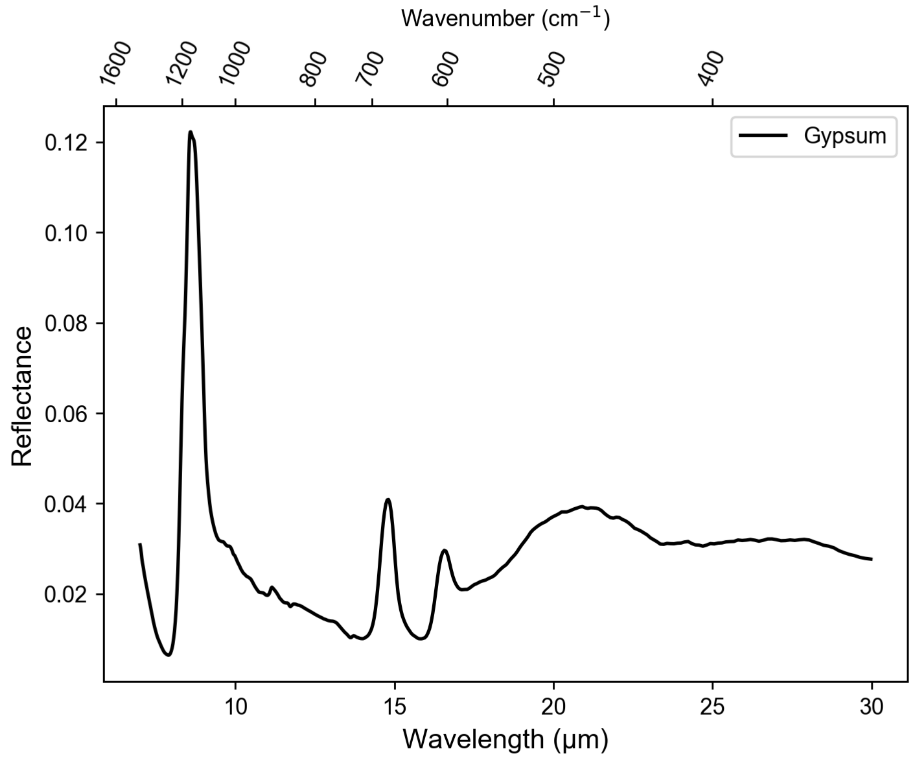

Figure 26: Gypsum FTIR Spectroscopy

2.6.4 VIS NIR Spectroscopy

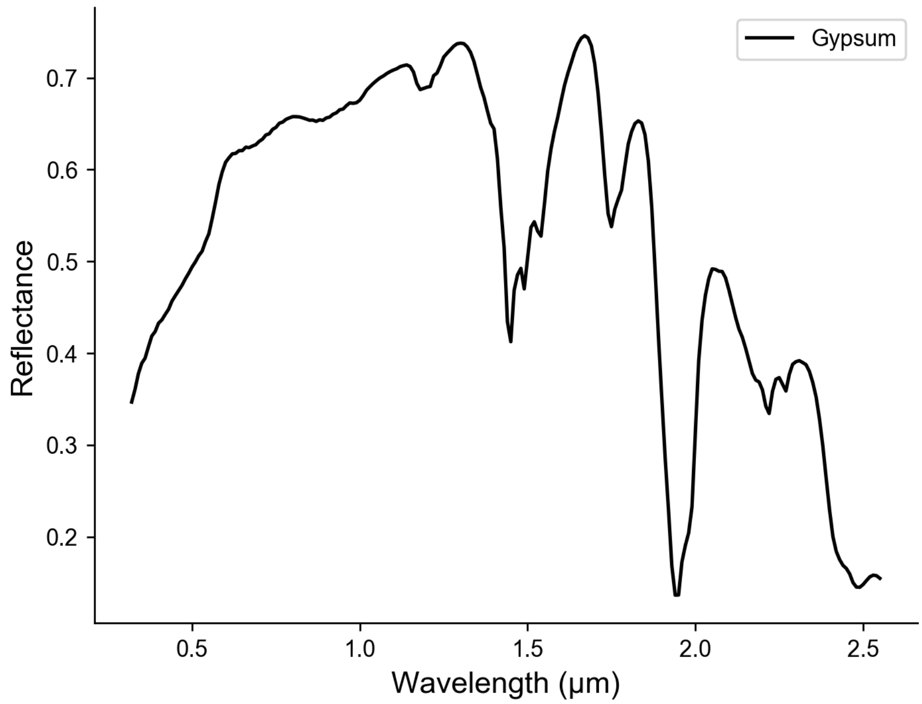

Figure 27: Gypsum FTIR Spectroscopy

2.6.5 Particle Size Analysis

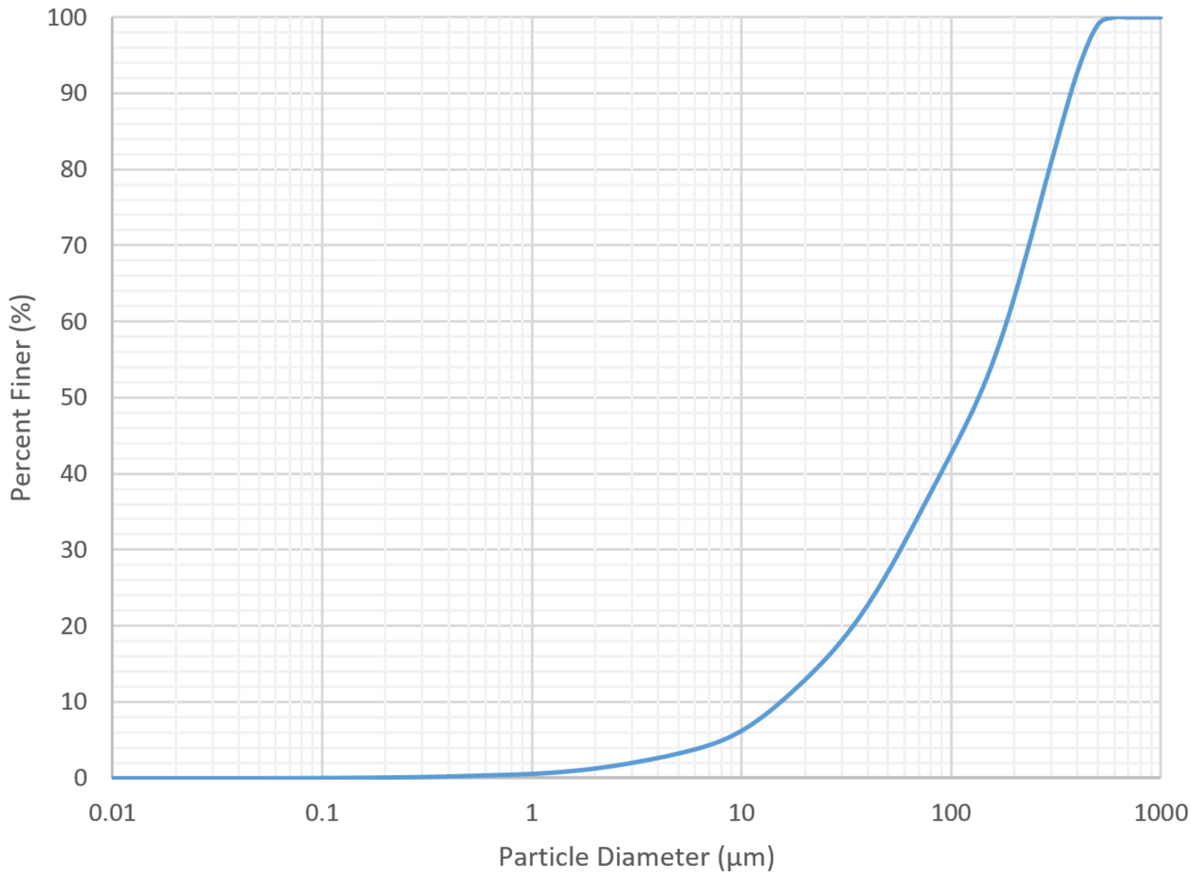

Figure 28: Gypsum Particle Size Distribution

2.7 Hematite

- Description: Iron oxide
- Source: Alpha Chemicals Red Iron Oxide
- Idealized Formula:Fe_2O_3
- Also called: Iron(III) oxide, red iron oxide

Notes Major phase confirmed by XRD analysis (Figure 30, Table 12). Additional peaks indicate the presence of a minor contaminant phase. XRF analysis (Table 13) shows 87.3 wt% iron oxide with an excess of SiO_2 (6.7 wt%) and Al_2O_3 (3.0 wt%), suggesting the presence of an aluminum silicate.

Figure 29: Photo of Hematite.

2.7.1 X-Ray Diffraction Pattern

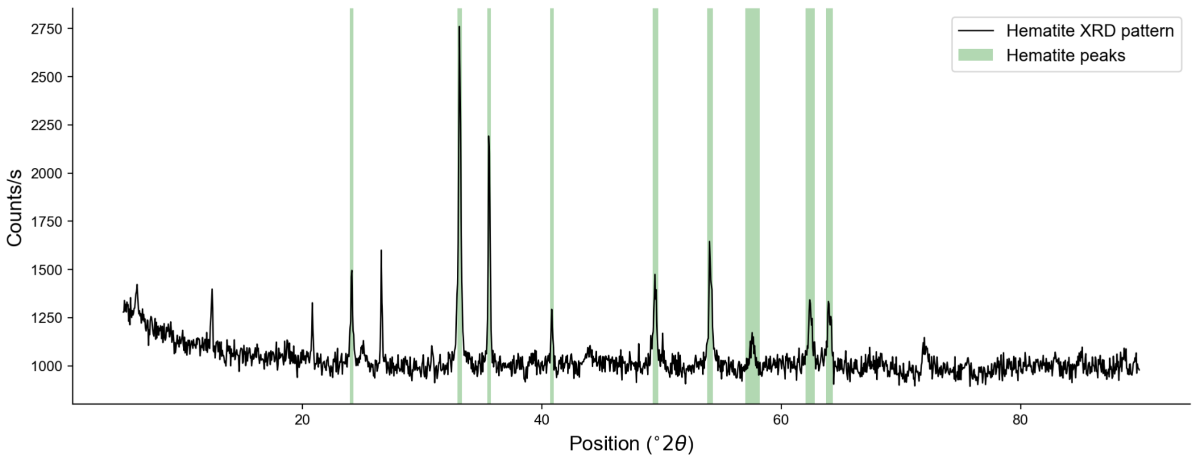

Figure 30: XRD Pattern for Hematite Sample.

Table 12: Hematite - XRD Pattern Peaks

Position (°2θ)	*Relative Intensity (%)*	*d-spacing (Å)*	*Matched By*
5.51	15.9	16.04	
12.42	19.4	7.12	
20.84	17.2	4.26	
24.11	30.8	3.69	Hematite
26.60	32.5	3.35	
33.14	100.0	2.70	Hematite
35.60	70.5	2.52	Hematite
40.85	16.9	2.21	Hematite
49.48	24.1	1.84	Hematite
54.04	37.3	1.70	Hematite
57.59	8.6	1.60	Hematite
62.43	19.8	1.49	Hematite
64.03	17.3	1.45	Hematite

Peak match citation: PDF 00-024-0072 in Gates-Rector and Blanton (2019)

2.7.2 Chemistry from X-Ray Fluorescence

Table 13: Hematite - Bulk Chemistry

Compound	*Concentration (wt%)*
Al_2O_3	3.0
SiO_2	6.7
P_2O_5	0.8
SO_3	0.1
Cl	0.1
K_2O	0.3
CaO	0.8
TiO_2	0.2
MnO	0.5
Fe_2O_3	87.3
NiO	0.1
HfO_2	< 0.1
Total	99.9

2.7.3 FTIR Spectroscopy

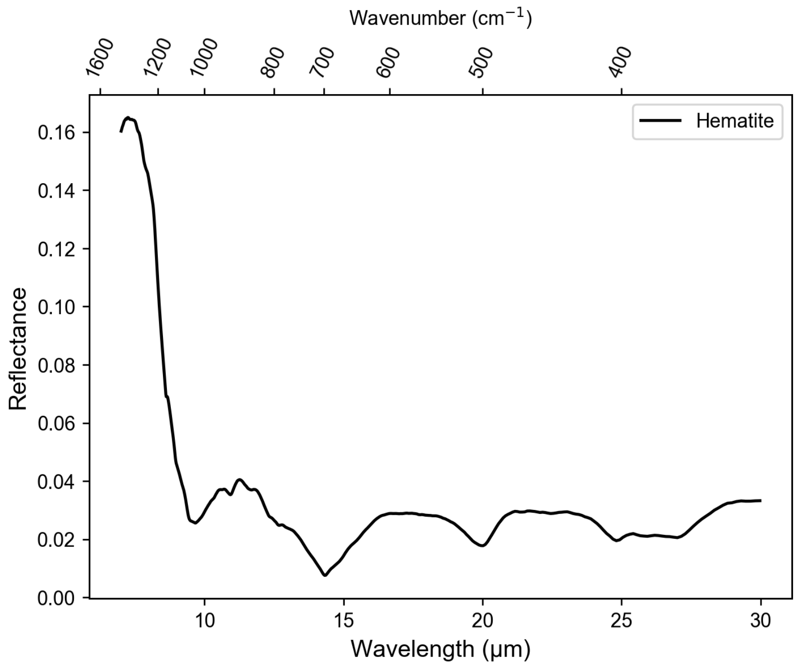

Figure 31: Hematite FTIR Spectroscopy

2.7.4 VIS NIR Spectroscopy

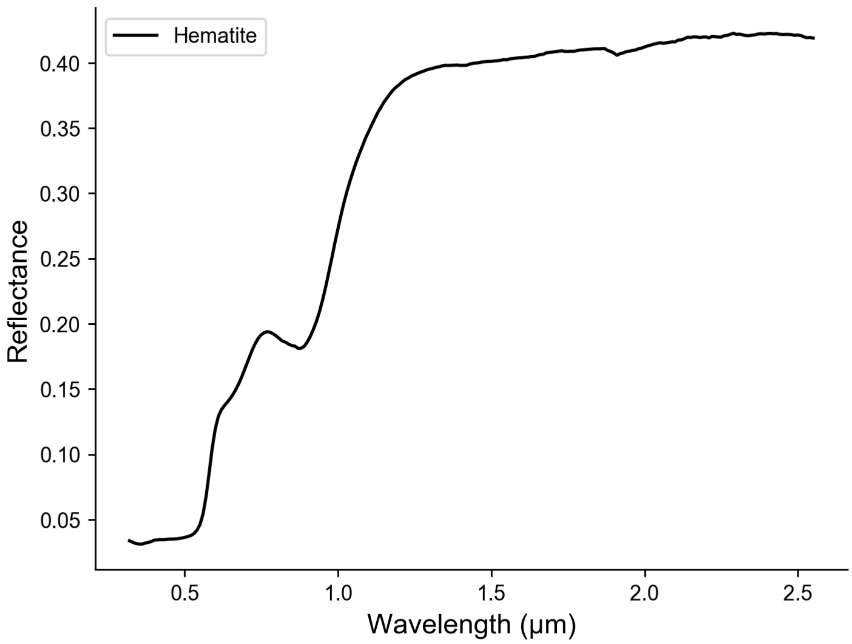

Figure 32: Hematite VIS NIR Spectroscopy

2.7.5 Particle Size Analysis

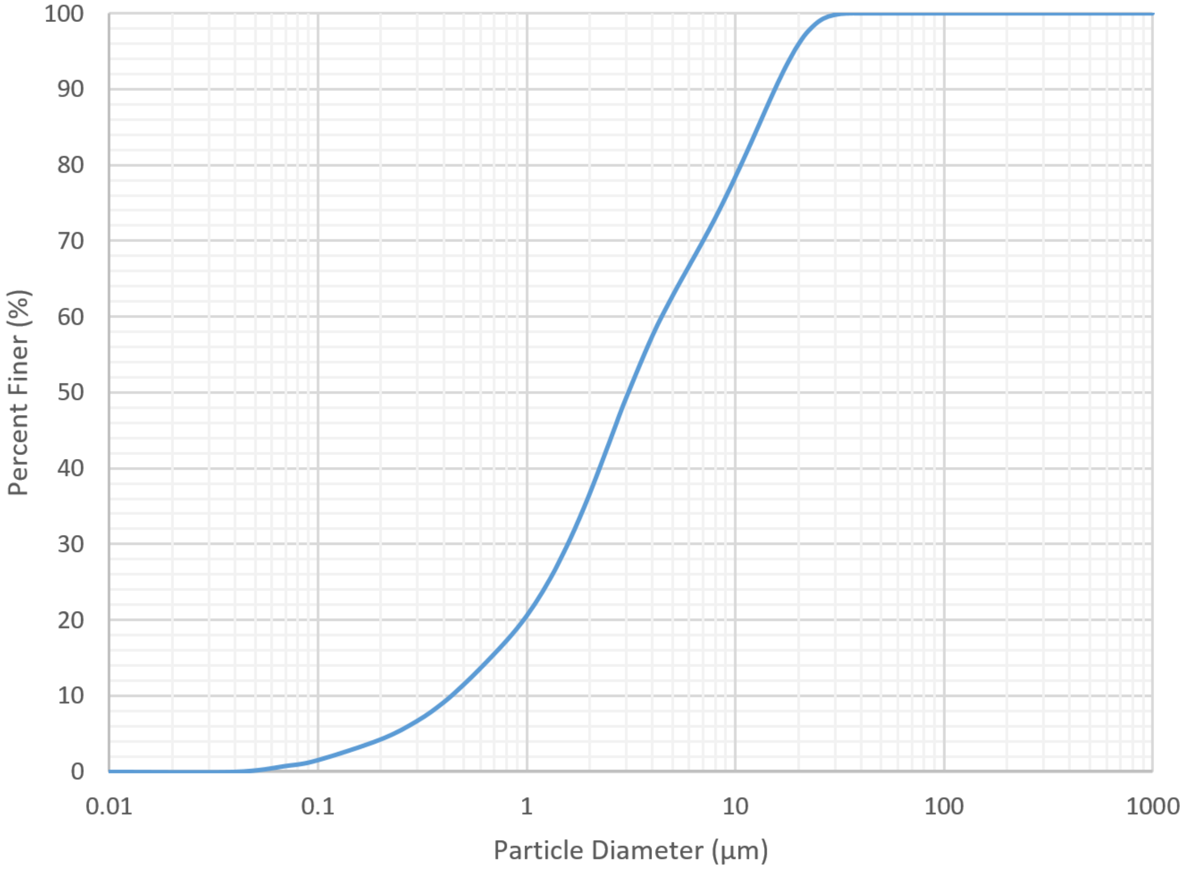

Figure 33: Hematite Particle Size Distribution

2.8 Ilmenite

- Description: Titanium iron oxide
- Source: Ceramic Supply, Inc. Ilmenite – Powder
- Idealized Formula: $FeTiO_3$
- Also called: Manaccanite

Notes XRD analysis (Figure 35, Table 14) shows the presence of both ilmenite and titanium(IV) oxide. The most intense peak in the XRD diffractogram at $2\theta = 54.2^{\circ}$ is associated with titanium(IV) oxide. XRF analysis (Table 15) shows concentration of 65.7 wt% TiO_2 and 26.9 wt% Fe_2O_3 with small amounts of MgO, Al_2O_3, and MnO.

Figure 34: Photo of ilmenite.

2.8.1 X-Ray Diffraction Pattern

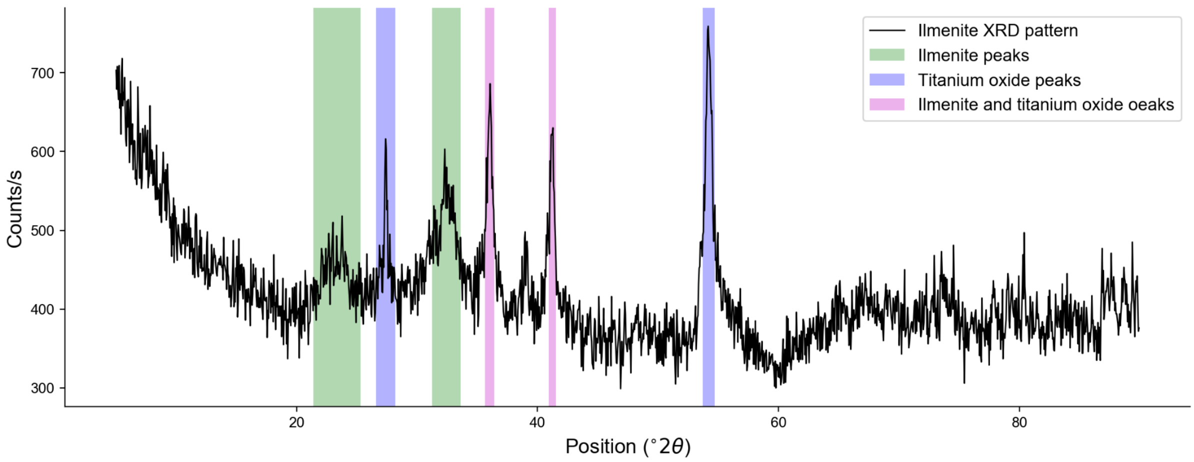

Figure 35: XRD Pattern for Ilmenite Sample.

Table 14: Ilmenite - XRD Pattern Peaks

Position (°2θ)	*Relative Intensity (%)*	*d-spacing (Å)*	*Matched By*
23.35	17.9	3.81	Ilmenite
27.40	42.8	3.26	Titanium oxide
32.43	47.3	2.76	Ilmenite
36.03	75.7	2.49	Ilmenite, titanium oxide
41.23	67.1	2.19	Ilmenite, titanium oxide
54.21	100.0	1.69	Titanium oxide

Peak match citation: PDF 01-080-2530 and PDF 01-070-6267 in Gates-Rector and Blanton (2019)

2.8.2 Chemistry from X-Ray Fluorescence

Table 15: Ilmenite - Bulk Chemistry

Compound	*Concentration (wt%)*
MgO	2.7
Al_2O_3	1.7
SiO_2	0.4
P_2O_5	0.8
CaO	0.2
TiO_2	65.7
Cr_2O_3	0.1
MnO	1.2
Fe_2O_3	26.9
Nb_2O_5	0.1
Total	99.9

2.8.3 FTIR Spectroscopy

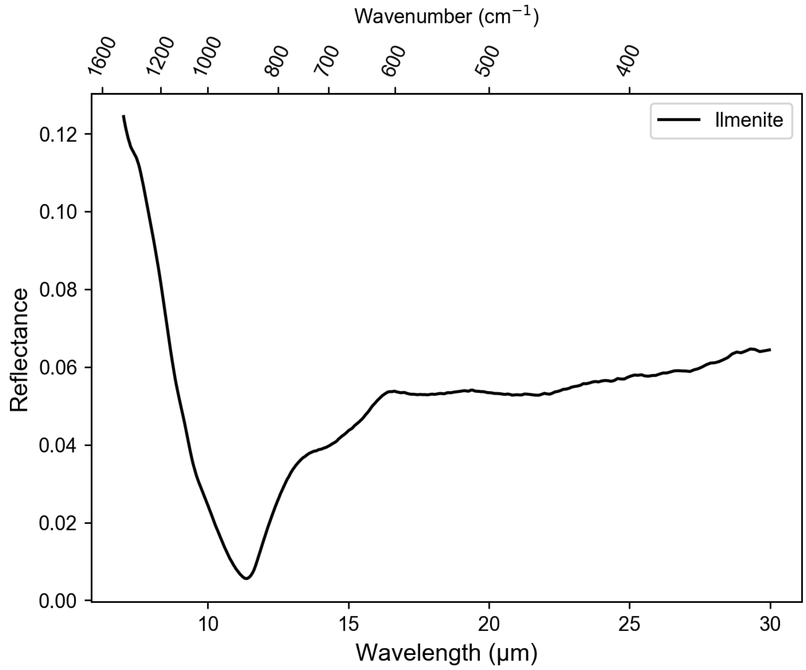

Figure 36: Ilmenite FTIR Spectroscopy

2.8.4 VIS NIR Spectroscopy

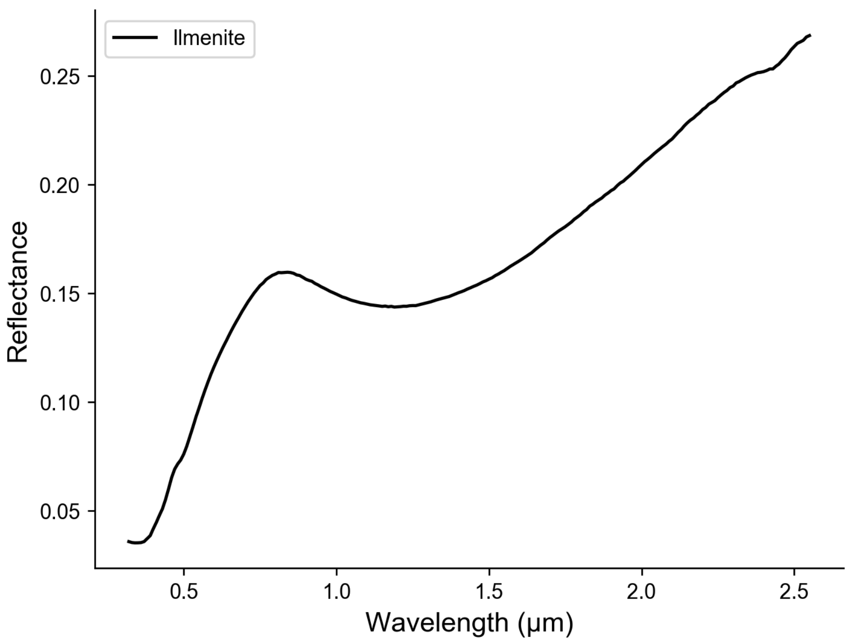

Figure 37: Ilmenite VIS NIR Spectroscopy

2.8.5 Particle Size Analysis

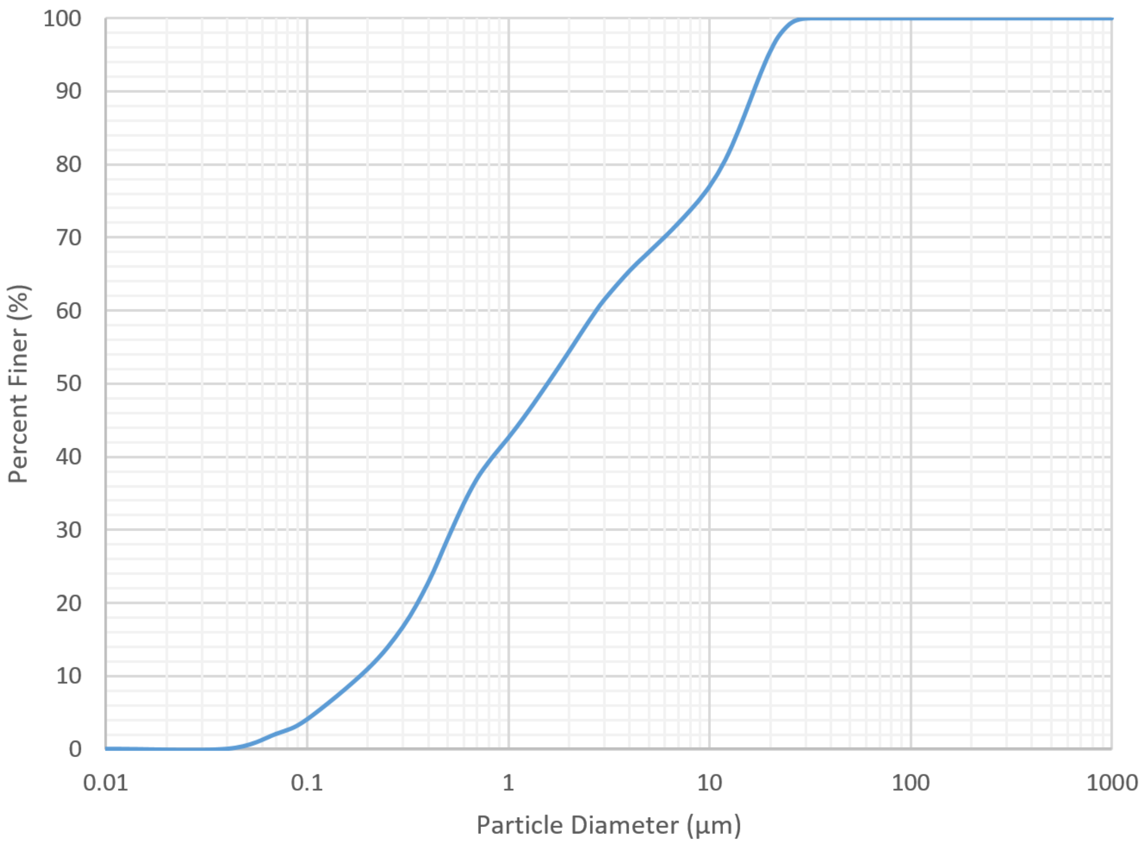

Figure 38: Ilmenite Particle Size Distribution

2.9 Magnesite

• Description: Magnesium carbonate

• Source: Reade

• Idealized Formula: $MgCO_3$

Notes Major phase confirmed by XRD analysis (Table 16, Figure 40). The MCF's XRF analyzer cannot detect carbon. The XRF data (Table 17) are otherwise consistent with magnesite as the main phase, with 69.3% MgO. There is some evidence of contamination from an aluminum silicate phase in the XRF data, but their relative concentrations would be lower if carbon could be detected and were included in the bulk chemistry quantification.

Figure 39: Photo of Magnesite.

2.9.1 X-Ray Diffraction Pattern

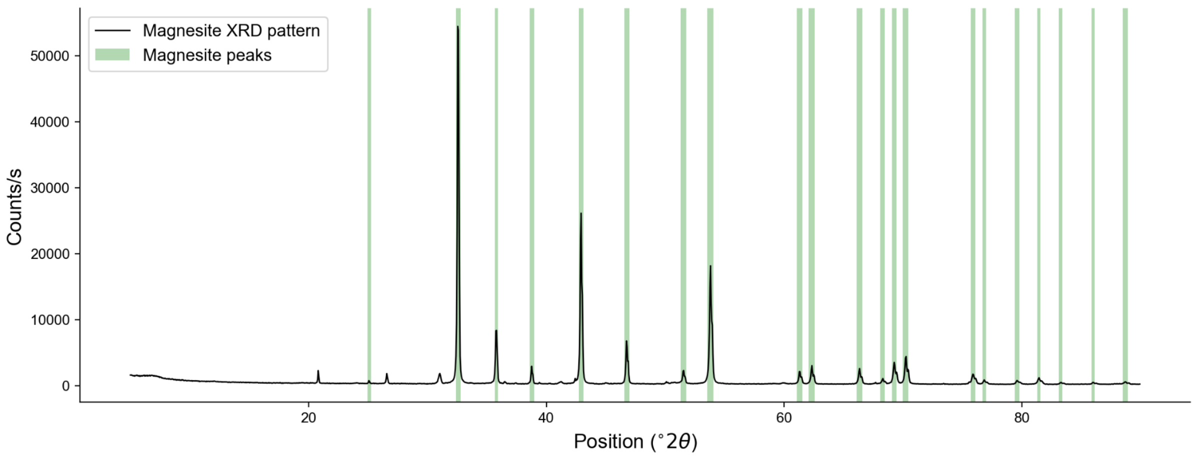

Figure 40: XRD Pattern for Magnesite Sample.

Table 16: Magnesite - XRD Pattern Peaks

Position (°2θ)	*Relative Intensity (%)*	*d-spacing (Å)*	*Matched By*
7.08	1.5	12.48	
20.83	3.3	4.27	
25.09	0.8	3.55	Magnesite
26.60	2.6	3.35	
31.04	2.8	2.88	
32.59	100.0	2.75	Magnesite
35.80	14.5	2.51	Magnesite
36.52	0.5	2.46	
38.79	4.4	2.32	Magnesite
41.23	0.6	2.19	
42.93	47.4	2.11	Magnesite
45.01	0.2	2.01	
46.77	11.0	1.94	Magnesite
51.54	3.7	1.77	Magnesite
53.79	30.8	1.70	Magnesite
59.95	0.3	1.54	
61.29	3.6	1.51	Magnesite
62.30	4.8	1.49	Magnesite
66.32	4.1	1.41	Magnesite
68.27	1.4	1.37	Magnesite
69.24	5.6	1.36	Magnesite
70.21	7.4	1.34	Magnesite
75.86	2.7	1.25	Magnesite
76.81	1.1	1.24	Magnesite
79.58	1.0	1.20	Magnesite
81.41	1.8	1.18	Magnesite
83.25	0.4	1.16	Magnesite
85.97	0.5	1.13	Magnesite
88.68	0.6	1.10	Magnesite

Peak match citation: PDF 01-071-1534 in Gates-Rector and Blanton (2019)

2.9.2 Chemistry from X-Ray Fluorescence

Table 17: Magnesite - Bulk Chemistry

Compound	*Concentration (wt%)*
MgO	69.3
Al_2O_3	0.8
SiO_2	11.6
P_2O_5	2.8
SO_3	1.4
Cl	1.9
CaO	11.2
Cr_2O_3	0.1
MnO	0.1
Fe_2O_3	0.6
NiO	0.3
Total	100.0

2.9.3 FTIR Spectroscopy

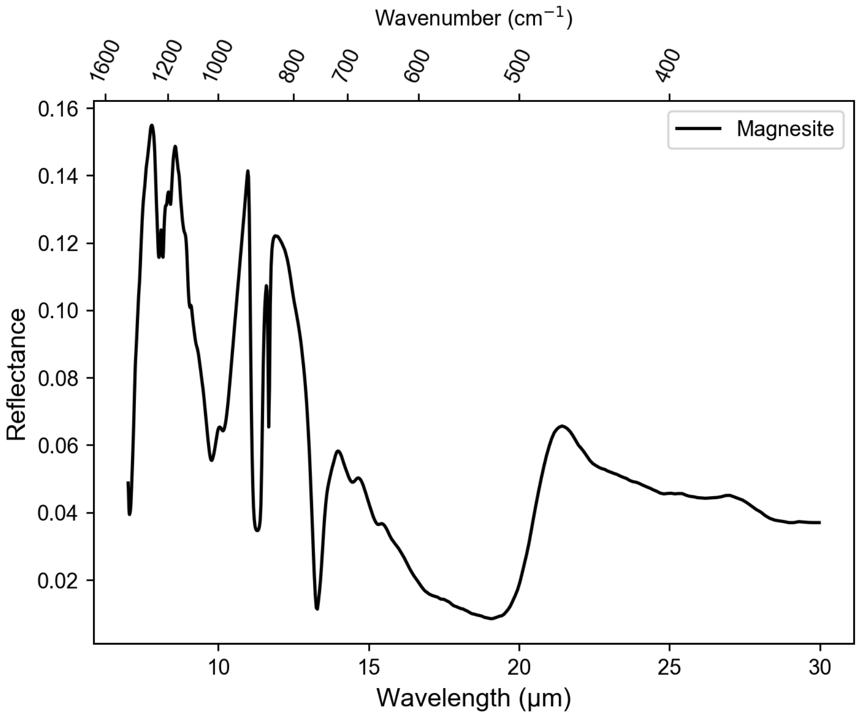

Figure 41: Magnesite FTIR Spectroscopy

2.9.4 VIS NIR Spectroscopy

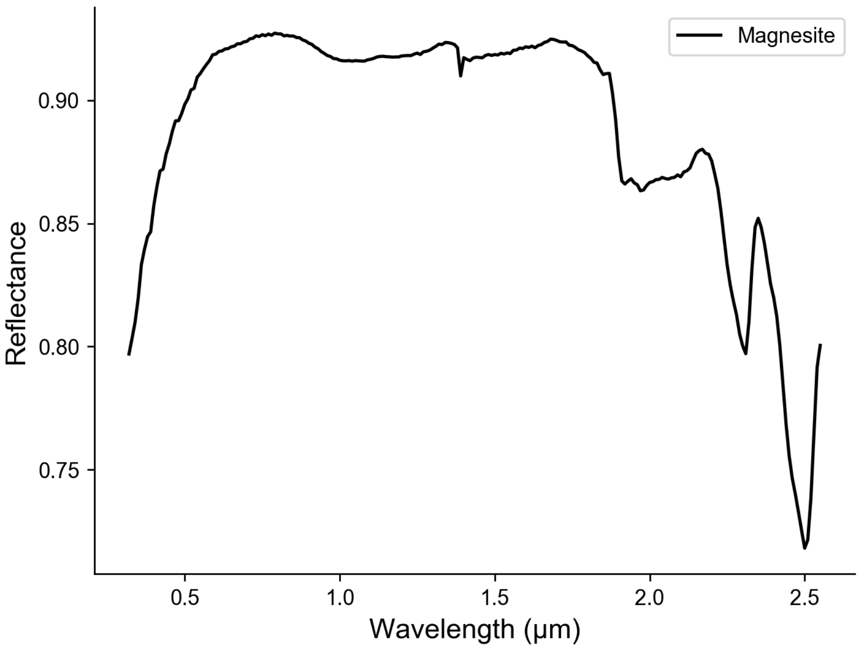

Figure 42: Magnesite VIS NIR Spectroscopy

2.9.5 Particle Size Analysis

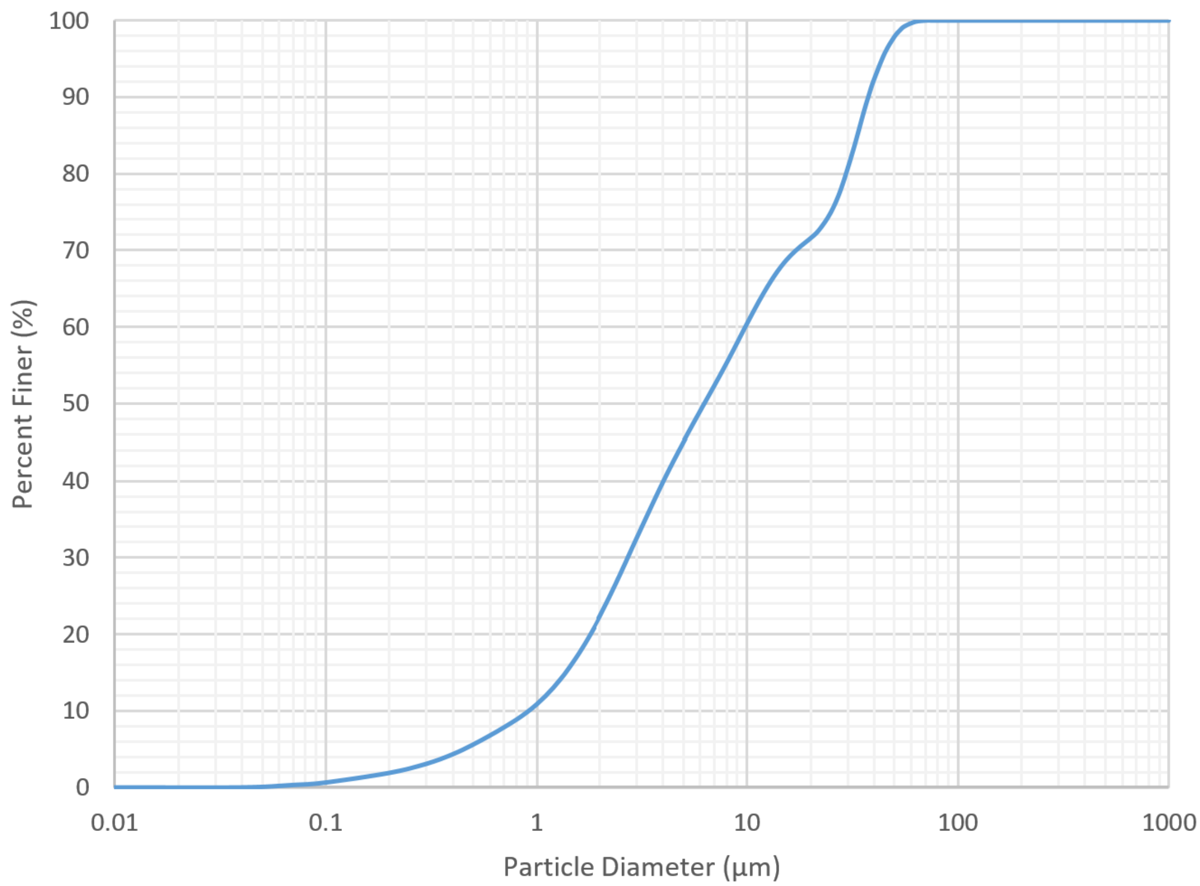

Figure 43: Magnesite Particle Size Distribution

2.10 Magnetite

- Description: Iron oxide
- Source: –
- Idealized Formula: Fe_3O_4
- Also called: Ferrous-ferric oxide

Notes XRD analysis (Table 18, Figure 45) confirms the major phase is magnetite. XRF analysis (Table 19) shows ~ 90% iron oxide content.

Figure 44: Photo of Magnetite.

2.10.1 X-Ray Diffraction Pattern

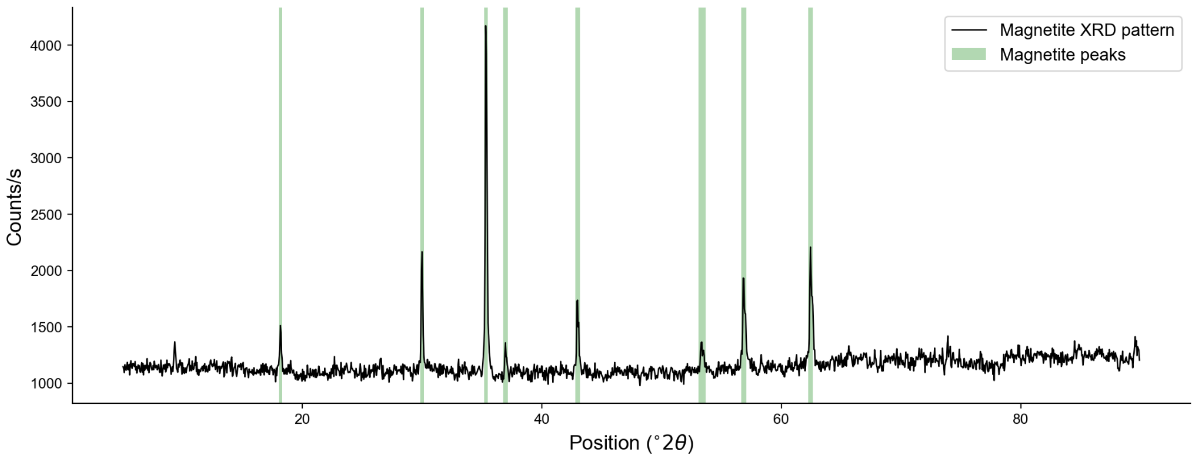

Figure 45: XRD Pattern for Magnetite Sample.

Table 18: Magnetite - XRD Pattern Peaks

Position (°2θ)	*Relative Intensity (%)*	*d-spacing (Å)*	*Matched By*
18.19	13.6	4.88	Magnetite
29.99	34.0	2.98	Magnetite
35.35	100.0	2.54	Magnetite
36.98	8.2	2.43	Magnetite
42.99	21.6	2.10	Magnetite
53.40	7.2	1.72	Magnetite
56.87	26.4	1.62	Magnetite
62.45	34.6	1.49	Magnetite
64.11	1.6	1.45	
80.43	2.0	1.19	

Peak match citation: PDF 01-071-6448 in Gates-Rector and Blanton (2019)

2.10.2 Chemistry from X-Ray Fluorescence

Table 19: Magnetite - Bulk Chemistry

Compound	*Concentration (wt%)*
MgO	4.2
Al_2O_3	0.1
SiO_2	2.9
P_2O_5	0.7
Cl	0.1
CaO	1.0
MnO	0.2
Fe_2O_3	90.7
Total	99.9

2.10.3 FTIR Spectroscopy

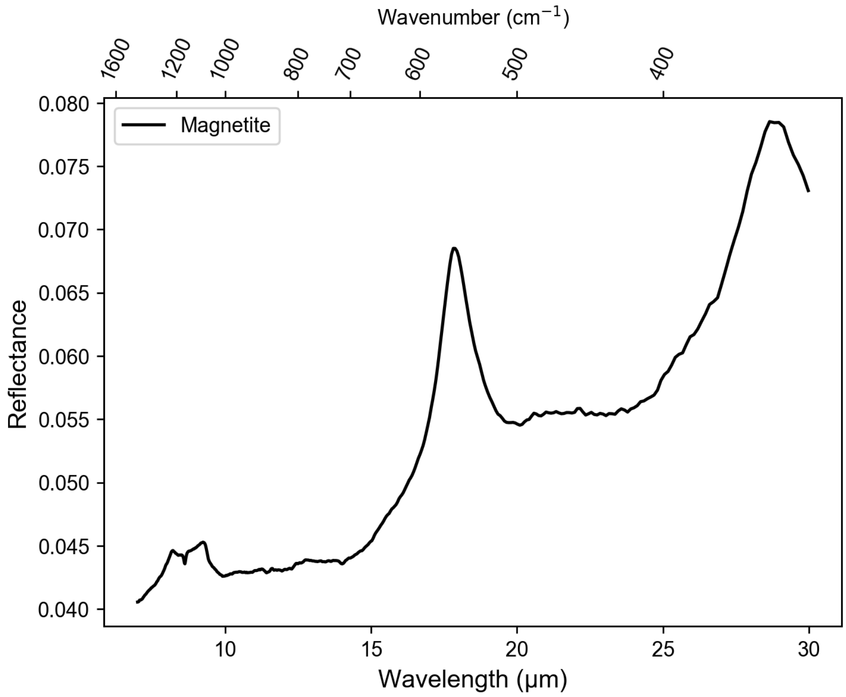

Figure 46: Magnetite FTIR Spectroscopy

2.10.4 VIS NIR Spectroscopy

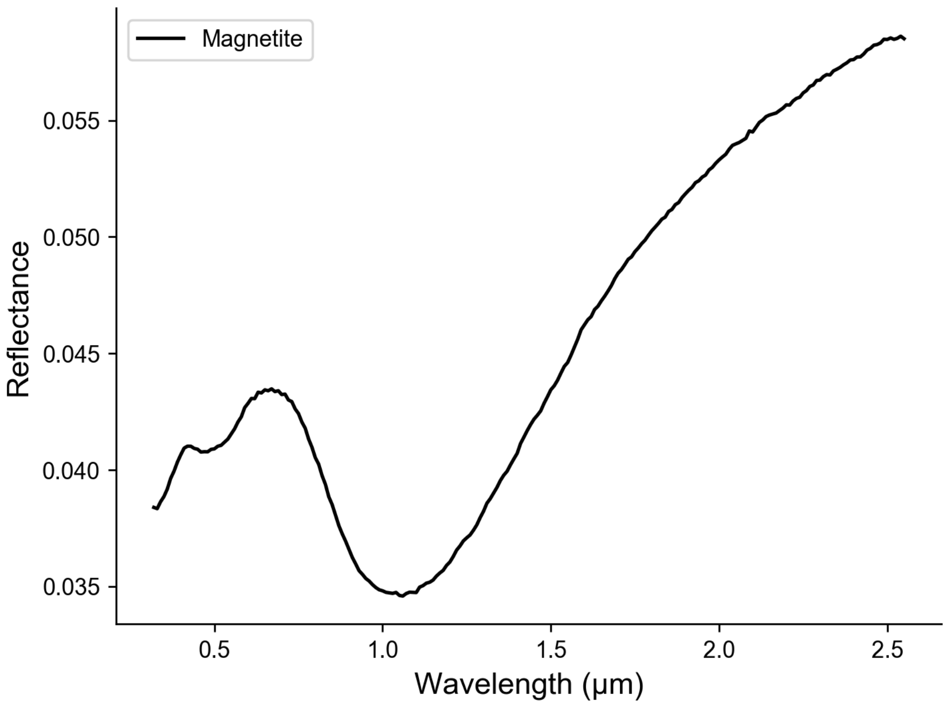

Figure 47: Magnetite VIS NIR Spectroscopy

2.10.5 Particle Size Analysis

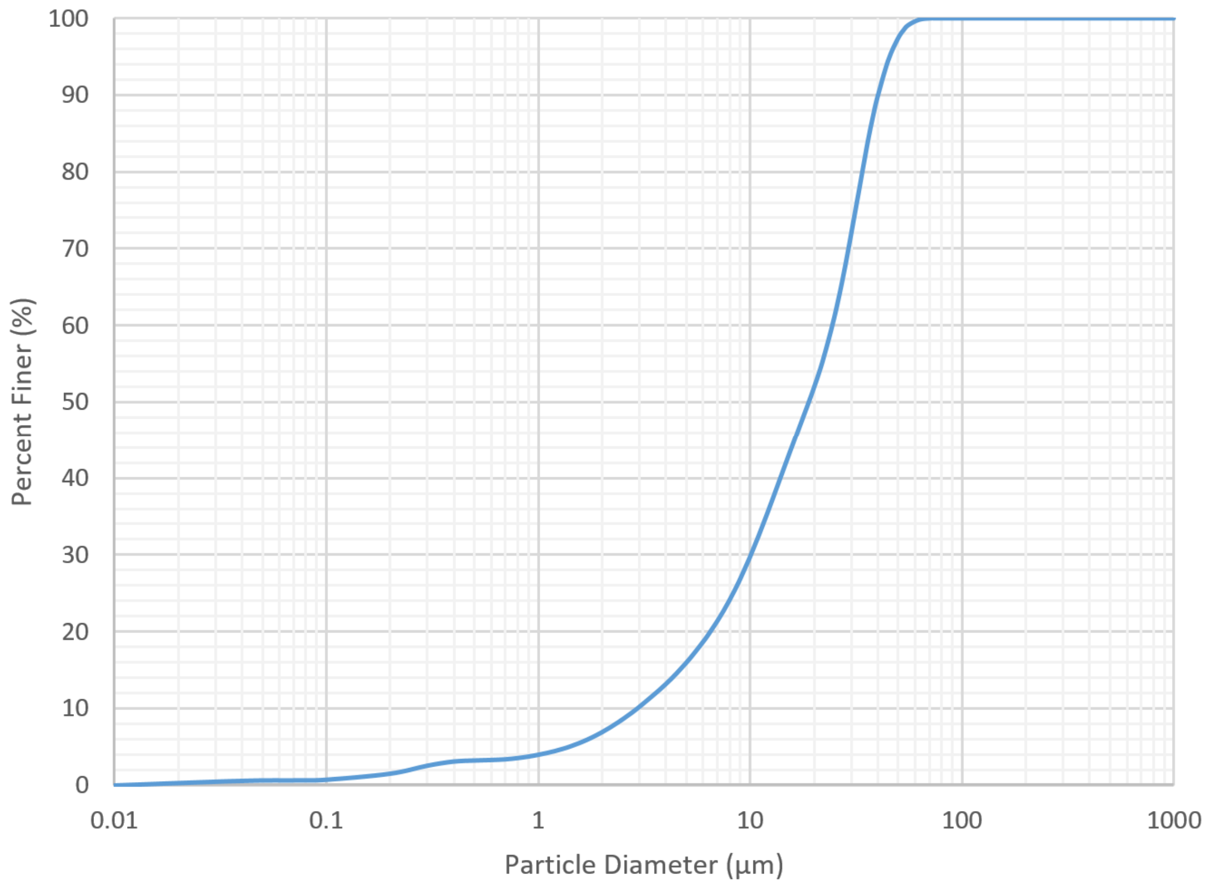

Figure 48: Magnetite Particle Size Distribution

2.11 Olivine

• Description: Nesosilicate mineral

• Source: United Western Supply

• Idealized Formula: $(Mg, Fe)_2SiO_4$

Notes Major phase confirmed by XRD analysis (Table 20, Figure 50). XRF analysis (Table 21) is consistent with a high fraction of Mg-rich olivine (forsterite).

Figure 49: Photo of olivine.

2.11.1 X-Ray Diffraction Pattern

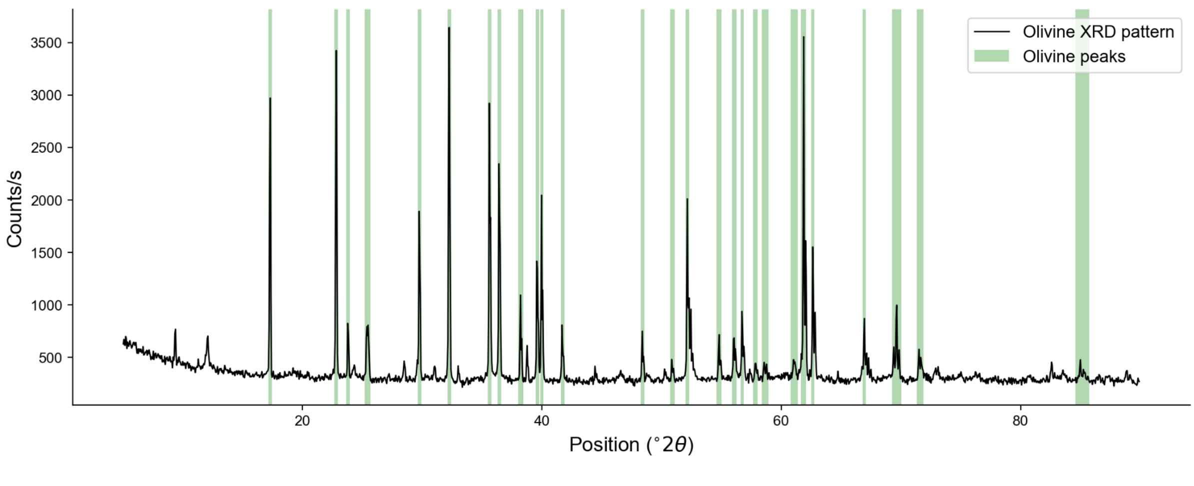

Figure 50: XRD pattern for olivine sample.

Table 20: Olivine - XRD Pattern Peaks

Position (°2θ)	*Relative Intensity (%)*	*d-spacing (Å)*	*Matched By*
9.37	9.6	9.44	
12.08	9.7	7.33	
17.30	74.2	5.13	Olivine ($Mg_{1.77}Fe_{0.23})SiO_4$)
22.82	100.0	3.90	Olivine ($Mg_{1.77}Fe_{0.23})SiO_4$)
23.82	15.6	3.74	Olivine ($Mg_{1.77}Fe_{0.23})SiO_4$)
25.43	14.0	3.50	Olivine ($Mg_{1.77}Fe_{0.23})SiO_4$)
28.50	5.5	3.13	
29.78	41.5	3.00	Olivine ($Mg_{1.77}Fe_{0.23})SiO_4$)
32.26	91.6	2.77	Olivine ($Mg_{1.77}Fe_{0.23})SiO_4$)
35.65	70.4	2.52	Olivine ($Mg_{1.77}Fe_{0.23})SiO_4$)
36.46	53.6	2.46	Olivine ($Mg_{1.77}Fe_{0.23})SiO_4$)
38.24	22.0	2.35	Olivine ($Mg_{1.77}Fe_{0.23})SiO_4$)
39.63	33.7	2.27	Olivine ($Mg_{1.77}Fe_{0.23})SiO_4$)
40.00	45.9	2.25	Olivine ($Mg_{1.77}Fe_{0.23})SiO_4$)
41.73	11.3	2.16	Olivine ($Mg_{1.77}Fe_{0.23})SiO_4$)
48.42	9.8	1.88	Olivine ($Mg_{1.77}Fe_{0.23})SiO_4$)
50.91	4.0	1.79	Olivine ($Mg_{1.77}Fe_{0.23})SiO_4$)
52.17	43.4	1.75	Olivine ($Mg_{1.77}Fe_{0.23})SiO_4$)
54.80	11.8	1.68	Olivine ($Mg_{1.77}Fe_{0.23})SiO_4$)
56.07	12.2	1.64	Olivine ($Mg_{1.77}Fe_{0.23})SiO_4$)
56.74	20.1	1.62	Olivine ($Mg_{1.77}Fe_{0.23})SiO_4$)
57.84	5.5	1.59	Olivine ($Mg_{1.77}Fe_{0.23})SiO_4$)
58.66	3.9	1.57	Olivine ($Mg_{1.77}Fe_{0.23})SiO_4$)
61.08	5.8	1.52	Olivine ($Mg_{1.77}Fe_{0.23})SiO_4$)
61.86	73.0	1.50	Olivine ($Mg_{1.77}Fe_{0.23})SiO_4$)
62.63	39.5	1.48	Olivine ($Mg_{1.77}Fe_{0.23})SiO_4$)
66.93	16.7	1.40	Olivine ($Mg_{1.77}Fe_{0.23})SiO_4$)
69.65	14.9	1.35	Olivine ($Mg_{1.77}Fe_{0.23})SiO_4$)
71.60	5.4	1.32	Olivine ($Mg_{1.77}Fe_{0.23})SiO_4$)
85.15	2.3	1.14	Olivine ($Mg_{1.77}Fe_{0.23})SiO_4$)

Peak match citation: PDF 01-075-6789 in Gates-Rector and Blanton (2019)

2.11.2 Chemistry from X-Ray Fluorescence

Table 21: Olivine - Bulk Chemistry

Compound	*Concentration (wt%)*
MgO	44.3
Al_2O_3	0.8
SiO_2	39.6
P_2O_5	1.0
Cl	0.4
CaO	0.4
Cr_2O_3	0.5
MnO	0.2
Fe_2O_3	12.1
NiO	0.7
Total	100.0

2.11.3 FTIR Spectroscopy

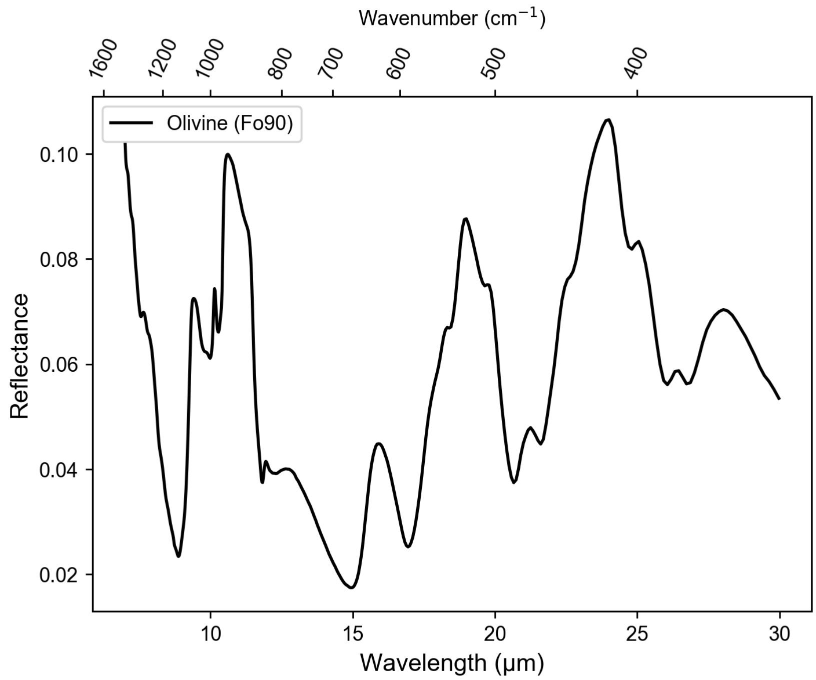

Figure 51: Olivine FTIR Spectroscopy

2.11.4 VIS NIR Spectroscopy

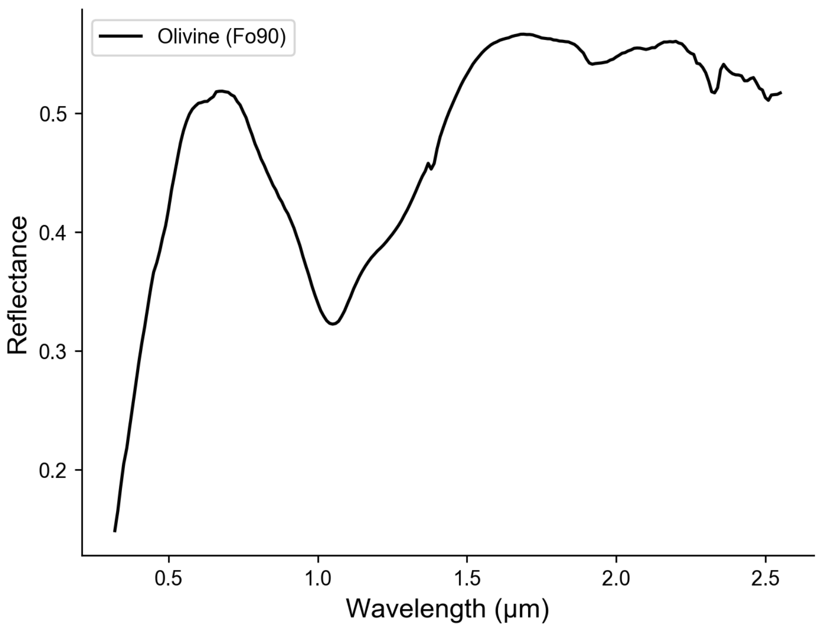

Figure 52: Olivine VIS NIR Spectroscopy

2.11.5 Particle Size Analysis

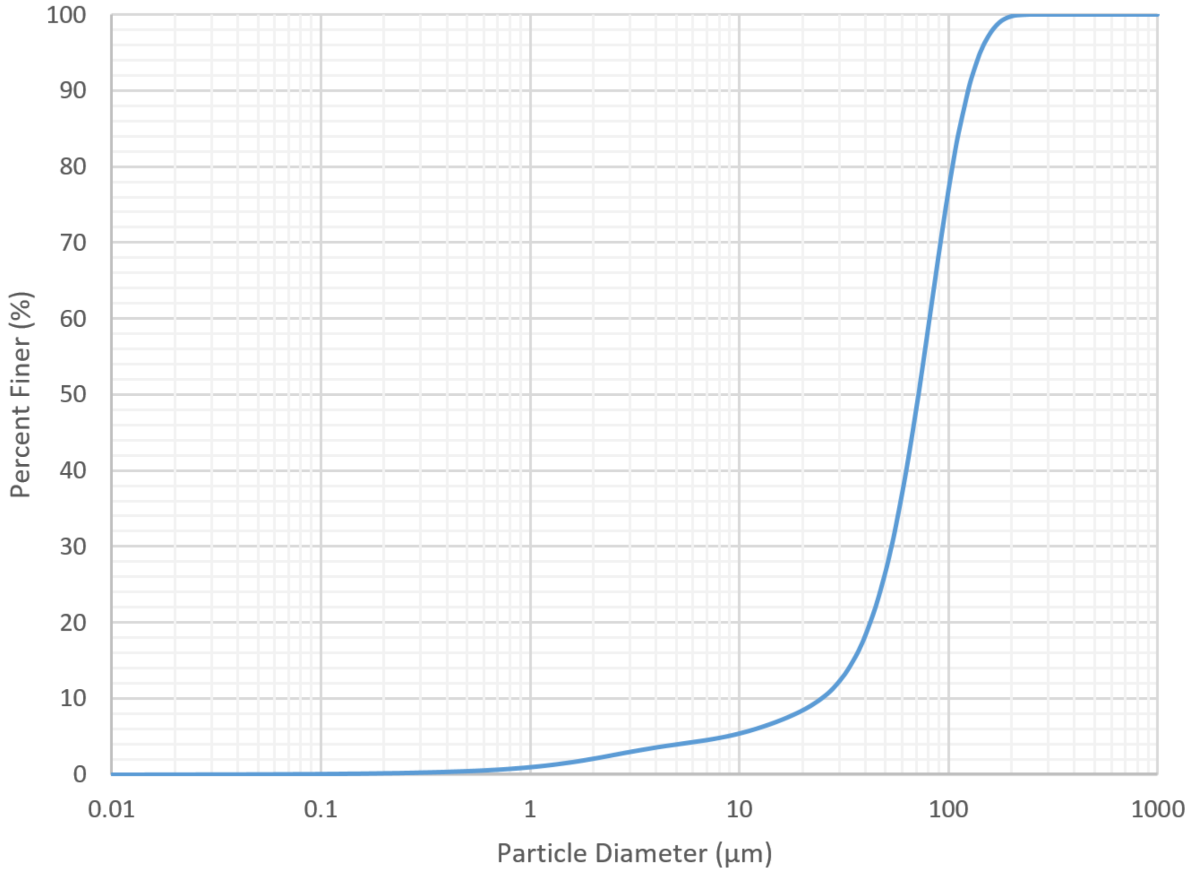

Figure 53: Olivine Particle Size Distribution

2.12 Pyrite

- Description: Iron sulfide
- Source: –
- Idealized Formula: FeS_2

Notes Major phase confirmed by XRD analysis (Table 22, Figure 55). XRF analysis (Table 23) shows ~ 90% of the mass is made up of iron and sulfur compounds.

Figure 54: Photo of Pyrite.

2.12.1 X-Ray Diffraction Pattern

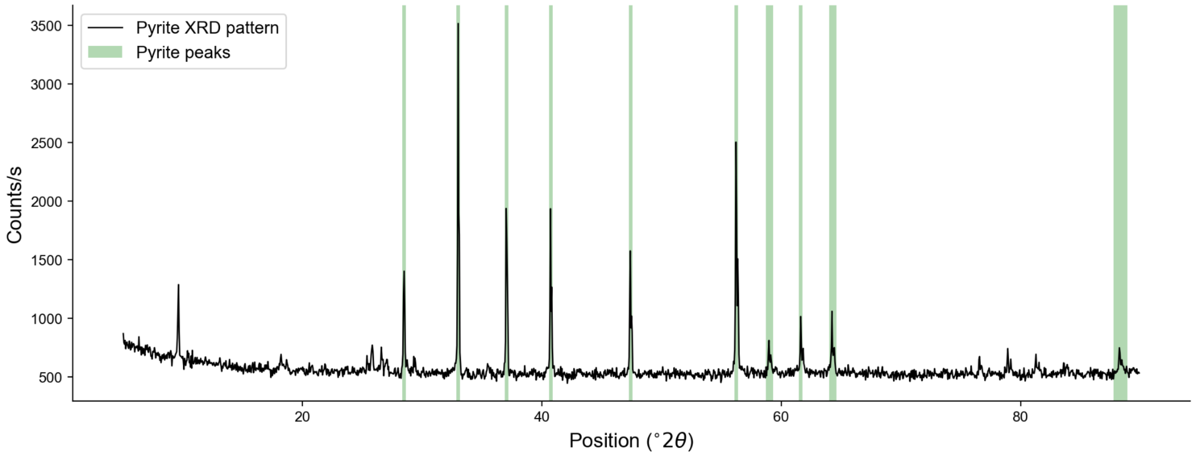

Figure 55: XRD Pattern for Pyrite Sample.

Table 22: Pyrite - XRD Pattern Peaks

Position (°2θ)	*Relative Intensity (%)*	*d-spacing (Å)*	*Matched By*
9.51	5.3	9.30	
18.37	2.2	4.83	
25.82	10.2	3.45	
28.49	37.3	3.13	Pyrite
33.03	100.0	2.71	Pyrite
37.07	51.7	2.43	Pyrite
40.75	52.0	2.21	Pyrite
47.41	30.0	1.92	Pyrite
56.24	82.9	1.64	Pyrite
59.03	8.3	1.56	Pyrite
61.63	21.7	1.50	Pyrite
64.30	12.0	1.45	Pyrite
88.34	5.8	1.11	Pyrite

Peak match citation: PDF 01-071-0053 in Gates-Rector and Blanton (2019)

2.12.2 Chemistry from X-Ray Fluorescence

Table 23: Pyrite - Bulk Chemistry

Compound	*Concentration (wt%)*
MgO	2.5
Al_2O_3	1.6
SiO_2	2.6
P_2O_5	0.5
SO_3	54.0
Cl	0.3
CaO	2.3
Fe_2O_3	35.7
CuO	0.4
ZnO	0.1
Total	100.0

2.12.3 FTIR Spectroscopy

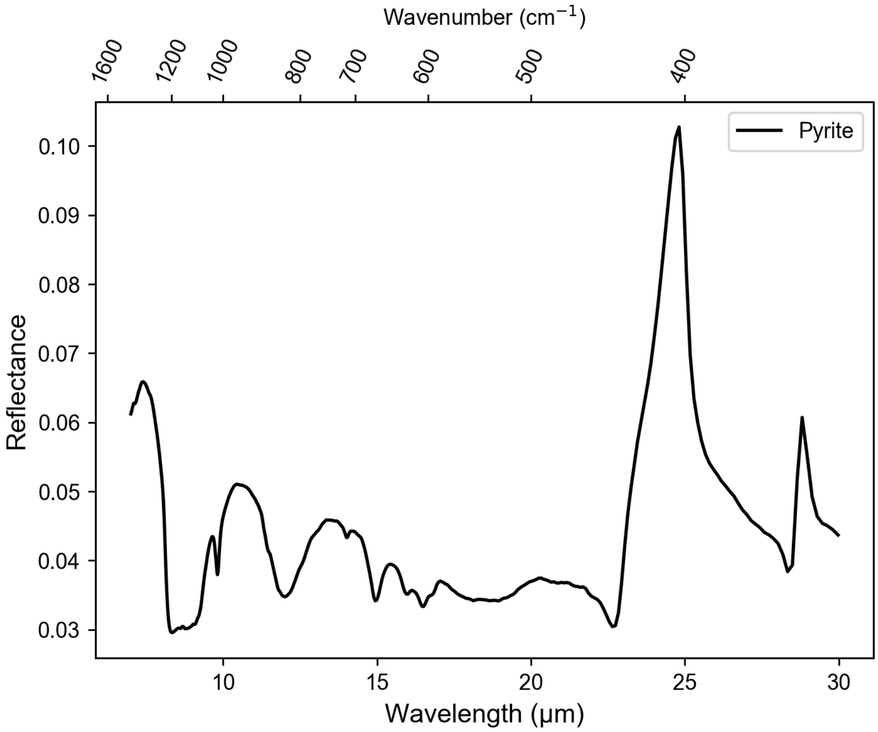

Figure 56: Pyrite FTIR Spectroscopy

2.12.4 VIS NIR Spectroscopy

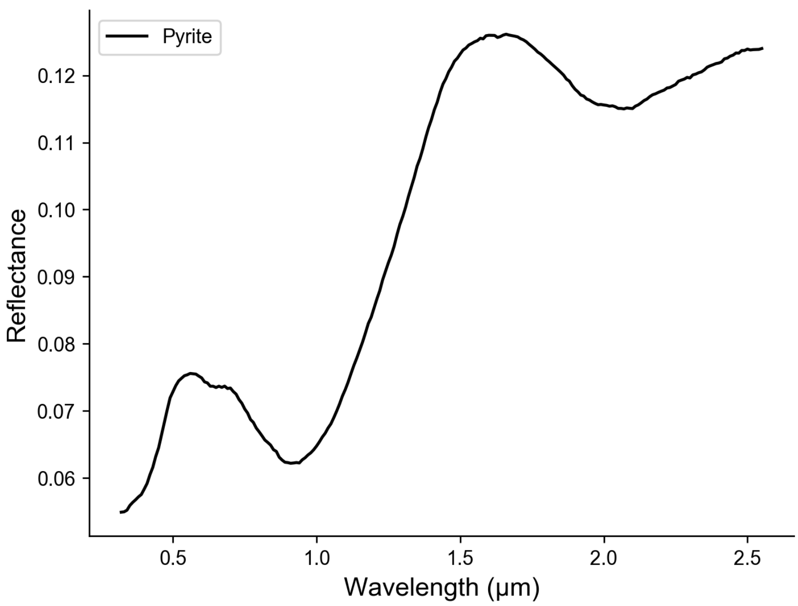

Figure 57: Pyrite VIS NIR Spectroscopy

2.12.5 Particle Size Analysis

Figure 58: Pyrite Particle Size Distribution

Coming Soon!

2.13 Siderite

- Description: Iron carbonate
- Source: SIDCO Minerals
- Idealized Formula: $FeCO_3$
- Also called: Iron(II) carbonate, ferric carbonate

Notes Major phase confirmed by XRD analysis (Table 24, Figure 60). XRF analysis (Table 25) shows 85% of the mass is made up of iron compounds. Carbon is too light to be detected with our XRF analyzer. There is some evidence of contamination from an aluminum silicate phase in the XRF data, but their relative concentrations would be lower if carbon could be detected and were included in the bulk chemistry quantification.

Figure 59: Photo of Siderite.

2.13.1 X-Ray Diffraction Pattern

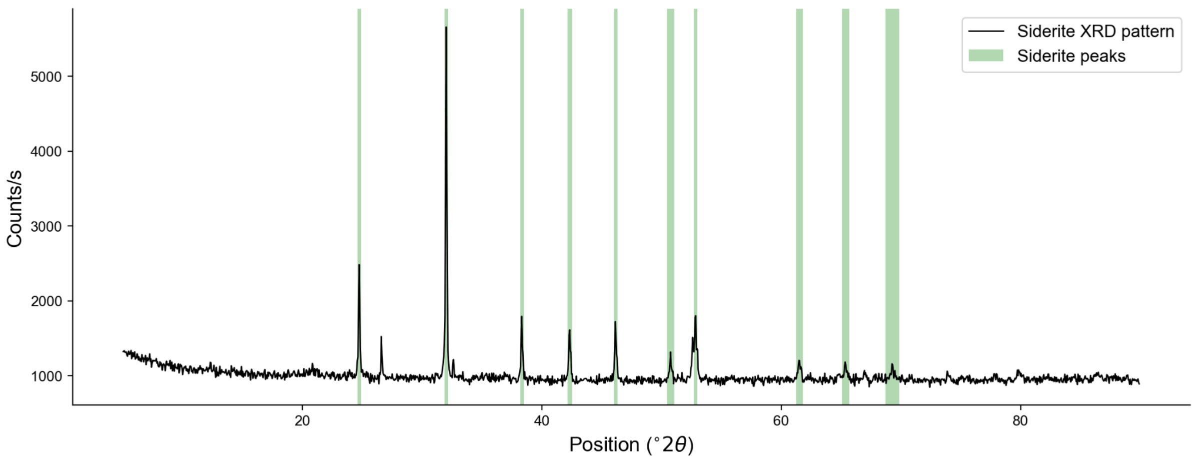

Figure 60: XRD Pattern for Siderite Sample.

Table 24: Siderite - XRD Pattern Peaks

Position (°2θ)	*Relative Intensity (%)*	*d-spacing (Å)*	*Matched By*
24.74	37.7	3.60	Siderite
26.62	9.7	3.35	
32.02	100.0	2.80	Siderite
38.33	19.9	2.35	Siderite
42.33	17.6	2.14	Siderite
46.17	16.9	1.97	Siderite
50.76	6.8	1.80	Siderite
52.84	22.0	1.73	Siderite
61.53	6.0	1.51	Siderite
65.40	4.7	1.43	Siderite
69.28	3.4	1.36	Siderite

Peak match citation: PDF 00-029-0696 in Gates-Rector and Blanton (2019)

2.13.2 Chemistry from X-Ray Fluorescence

Table 25: Siderite - Bulk Chemistry

Compound	*Concentration (wt%)*
Al_2O_3	5.0
SiO_2	7.0
P_2O_5	0.9
SO_3	0.4
Cl	0.2
K_2O	0.3
CaO	0.6
TiO_2	0.2
MnO	0.2
Fe_2O_3	85.0
ZnO	0.1
Rb_2O	0.2
Total	99.9

2.13.3 FTIR Spectroscopy

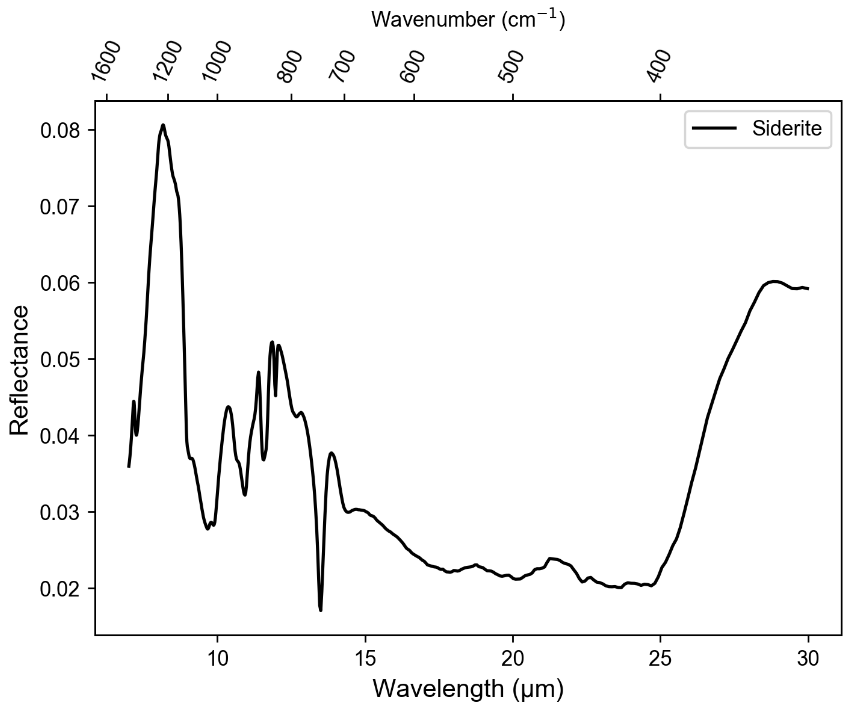

Figure 61: Siderite FTIR Spectroscopy

2.13.4 VIS NIR Spectroscopy

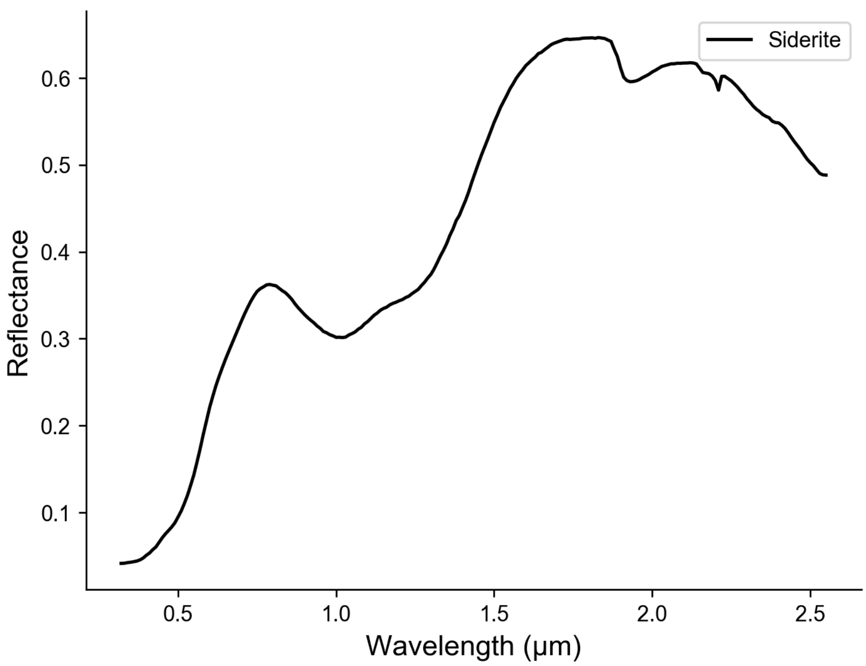

Figure 62: Siderite VIS NIR Spectroscopy

2.13.5 Particle Size Analysis

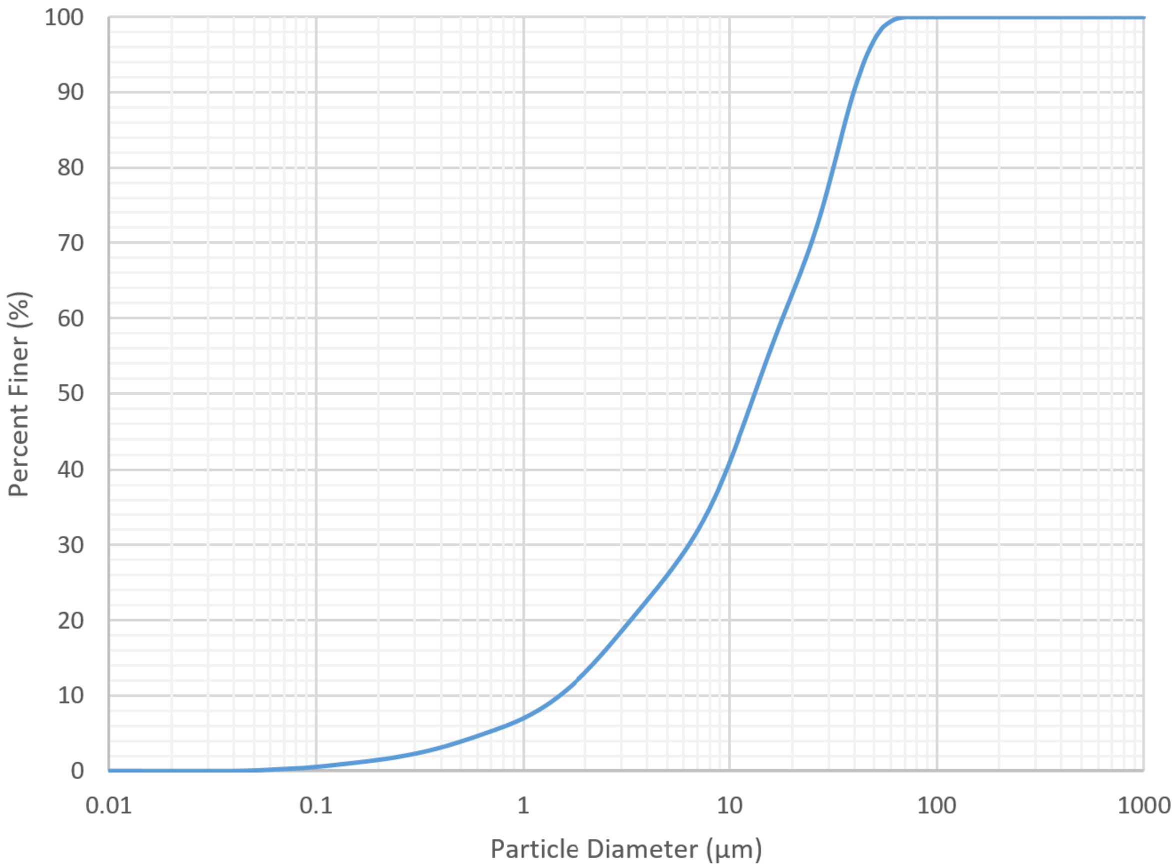

Figure 63: Siderite Particle Size Distribution

2.14 Smectite

- Description: Family of clay minerals
- Source: Aardvark Clay & Supplies (Bentonite, IBEX 200)
- Idealized Formula: $(Na,Ca)_{0.33}(Al,Mg)_2(Si_4O_{10})(OH)2 \cdot nH_2O$ (Montmorillonite, the primary phase in bentonite clay)

Notes XRD analysis confirms the major phases are the smectite-family clays nontronite and montmorillonite (Table 26, Figure 65). Other clays (kaolin and vermiculite) were also detected by XRD, and there were some unidentified XRD peaks. XRF analysis (Table 27) is consistent with primary phases of aluminum, magnesium, calcium, and/or iron silicates.

Figure 64: Photo of Smectite.

2.14.1 X-Ray Diffraction Pattern

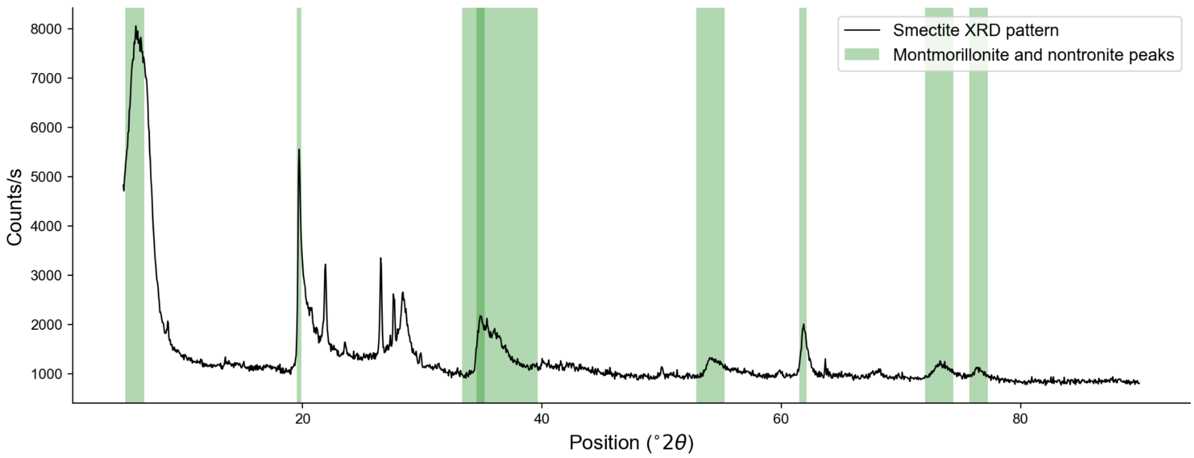

Figure 65: XRD Pattern for Smectite Sample.

Table 26: Smectite - XRD Pattern Peaks

Position (°2θ)	*Relative Intensity (%)*	*d-spacing (Å)*	*Matched By*
5.99	100.0	14.76	Montmorillonite, nontronite, vermiculite
7.00	85.6	12.63	Kaolin
19.71	66.3	4.51	Montmorillonite, nontronite, kaolin, vermiculite
21.92	32.6	4.06	
23.56	8.2	3.78	Vermiculite
26.55	34.8	3.36	
27.64	23.0	3.23	
28.37	24.6	3.15	Montmorillonite, vermiculite
34.87	17.8	2.57	Montmorillonite, nontronite, kaolin, vermiculite
36.49	9.4	2.46	Montmorillonite, nontronite, vermiculite
41.98	2.5	2.15	
54.08	5.3	1.70	Montmorillonite, nontronite, kaolin, vermiculite
61.82	15.1	1.50	Montmorillonite, nontronite, kaolin, vermiculite
68.04	2.2	1.38	
73.19	4.9	1.29	Montmorillonite, nontronite, kaolin, vermiculite
76.48	3.8	1.25	Montmorillonite, nontronite, kaolin, vermiculite

Peak match citation: PDF 00-002-0009, PDF 00-002-0017, PDF 00-002-0037, PDF 00-003-0009, and PDF 00-003-0010 in Gates-Rector and Blanton (2019)

2.14.2 Chemistry from X-Ray Fluorescence

Table 27: Smectite - Bulk Chemistry

Compound	*Concentration (wt%)*
MgO	1.8
Al_2O_3	20.3
SiO_2	65.8
P_2O_5	1.1
SO_3	1.1
Cl	0.4
K_2O	0.7
CaO	2.0
TiO_2	0.3
Fe_2O_3	6.5
SrO	0.1
Total	99.9

2.14.3 FTIR Spectroscopy

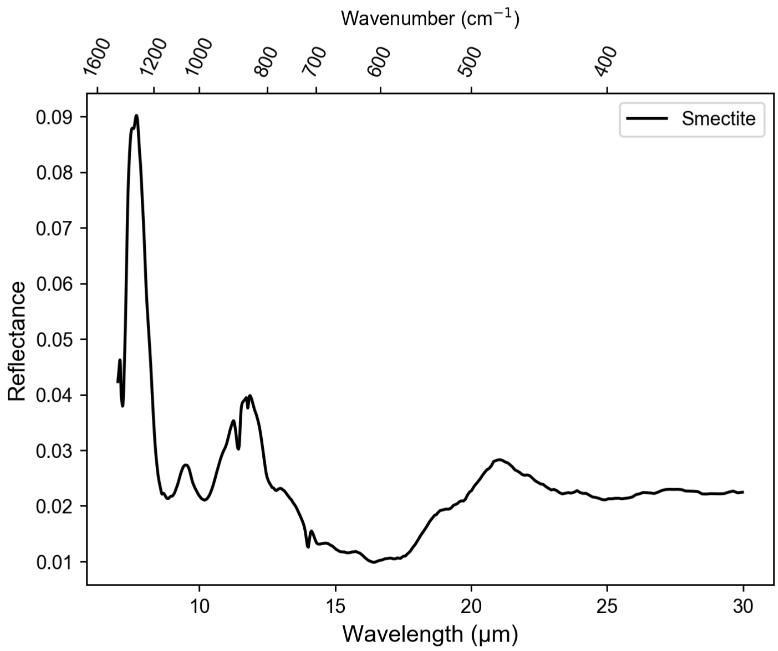

Figure 66: Smectite FTIR Spectroscopy

2.14.4 VIS NIR Spectroscopy

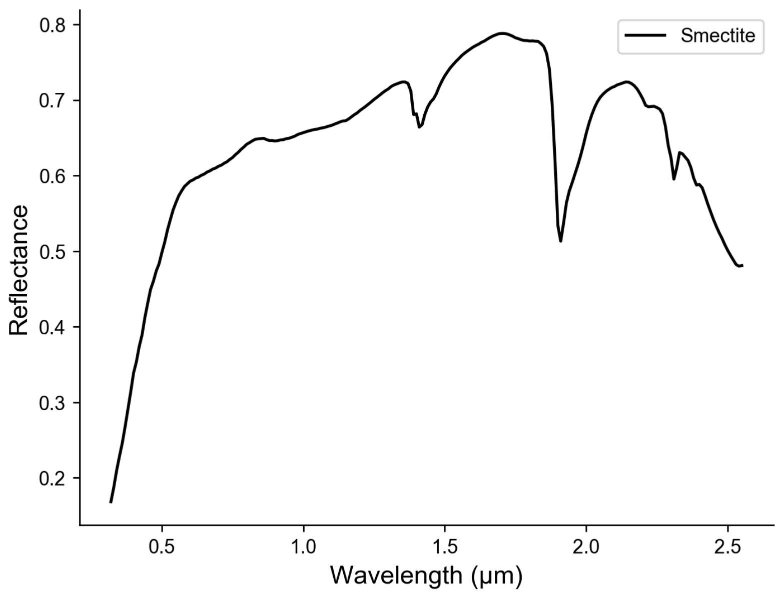

Figure 67: Smectite VIS NIR Spectroscopy

2.14.5 Particle Size Analysis

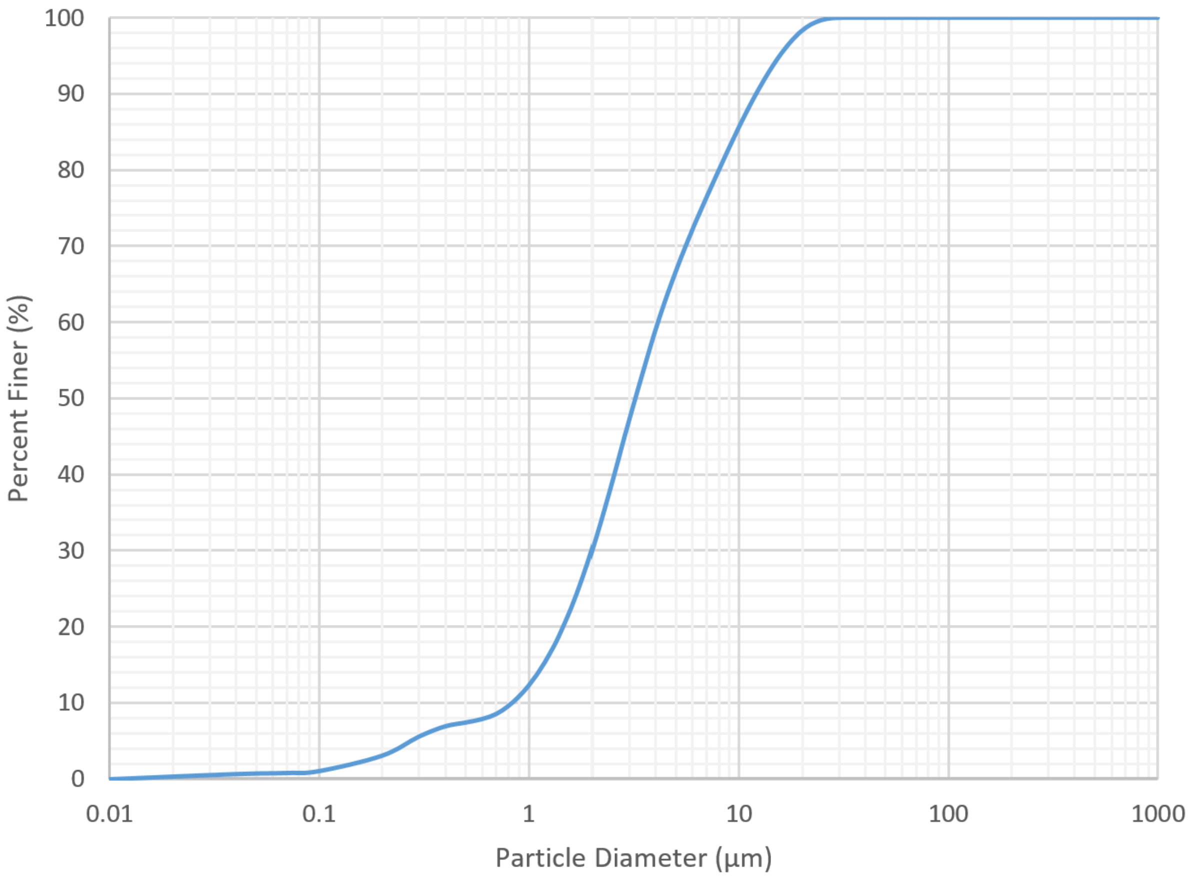

Figure 68: Smectite Particle Size Distribution

2.15 Vermiculite

• Description: Phyllosilicate

• Source: –

• Idealized Formula: $(Mg,Fe^{2+},Fe^{3+})_3[(Al,Si)_4O_{10}](OH)_2 \cdot 4H_2O$

Notes XRD analysis confirms vermiculite is the major phase (Table 28, Figure 70). XRF analysis (Table 29) is consistent with a primary phase of aluminum, magnesium, and/or iron silicates. Vermiculite is a weathering product of muscovite, an aluminum-potassium phyllosilicate mineral. The detection of K_2O (6.7 wt%) in the XRF data is consistent with the presence of some muscovite.

Figure 69: Photo of Vermiculite.

2.15.1 X-Ray Diffraction Pattern

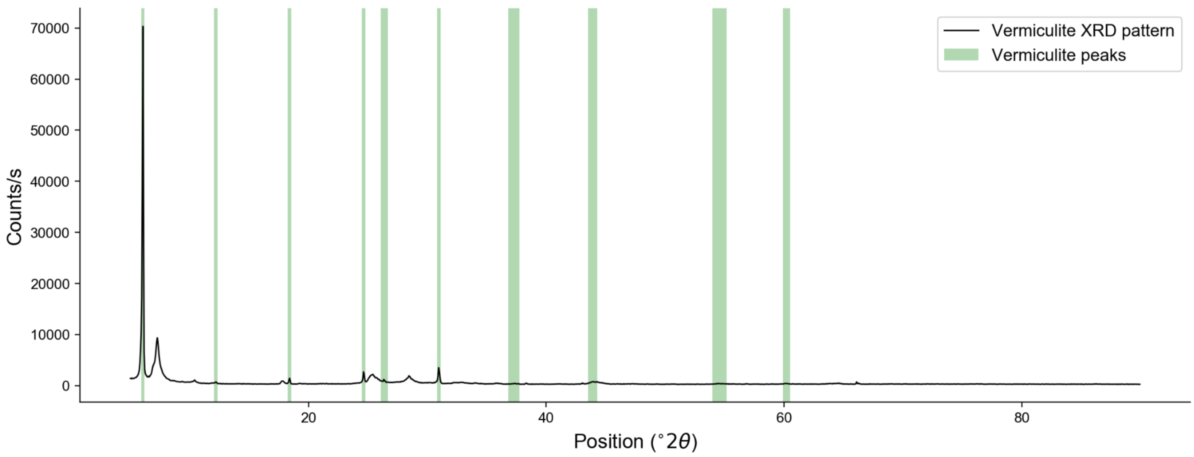

Figure 70: XRD pattern for vermiculite sample.

Table 28: Vermiculite - XRD Pattern Peaks

Position (°2θ)	*Relative Intensity (%)*	*d-spacing (Å)*	*Matched By*
6.08	100.0	14.54	Vermiculite
7.29	13.2	12.12	
10.43	1.1	8.49	
12.22	0.6	7.24	Vermiculite
17.80	0.9	4.98	
18.41	1.5	4.82	Vermiculite
24.65	3.5	3.61	Vermiculite
25.39	2.8	3.51	
26.38	1.1	3.38	Vermiculite
28.48	2.3	3.13	
30.97	4.2	2.89	Vermiculite
32.66	0.5	2.74	
35.85	0.2	2.50	
37.27	0.1	2.41	Vermiculite
38.32	0.2	2.35	
43.90	0.7	2.06	Vermiculite
54.56	0.2	1.68	Vermiculite
60.19	0.2	1.54	Vermiculite
64.51	0.2	1.44	
66.09	0.5	1.41	

Peak match citation: PDF 00-060-0341 in Gates-Rector and Blanton (2019)

2.15.2 Chemistry from X-Ray Fluorescence

Table 29: Vermiculite - Bulk Chemistry

Compound	*Concentration (wt%)*
MgO	14.5
Al_2O_3	12.4
SiO_2	36.2
P_2O_5	1.2
SO_3	0.3
Cl	0.5
K_2O	6.7
CaO	3.1
TiO_2	2.9
Cr_2O_3	0.2
MnO	0.2
Fe_2O_3	20.8
NiO	0.1
Rb_2O	0.1
SrO	0.1
BaO	0.5
Total	99.9

2.15.3 FTIR Spectroscopy

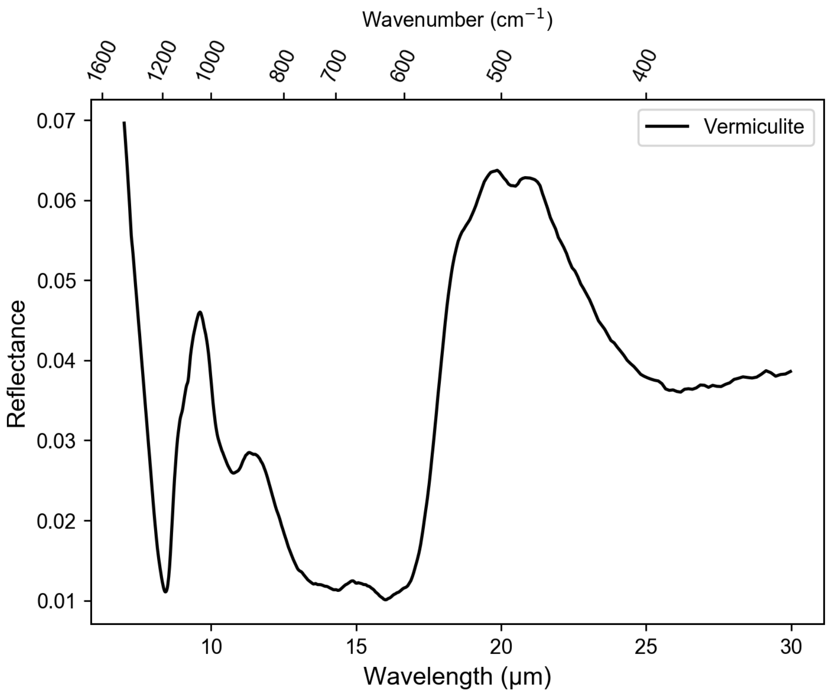

Figure 71: Vermiculite FTIR Spectroscopy

2.15.4 VIS NIR Spectroscopy

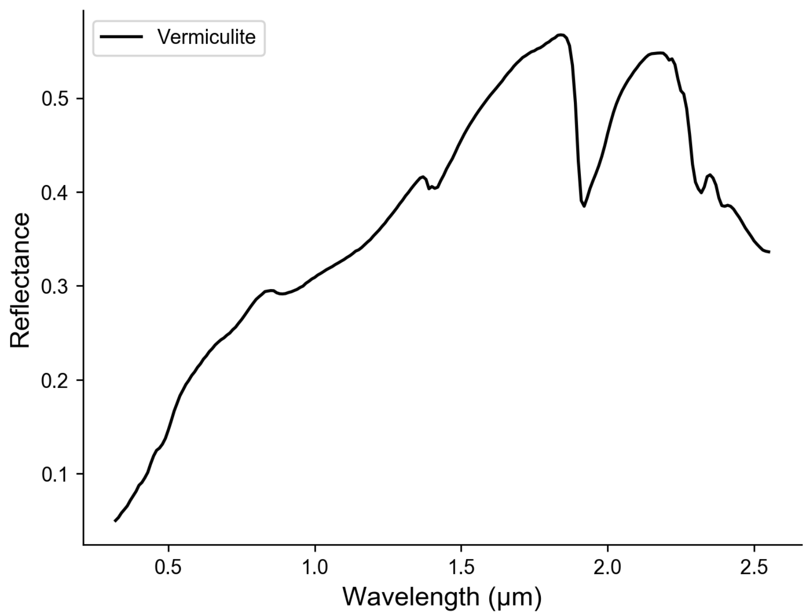

Figure 72: Vermiculite VIS NIR Spectroscopy

2.15.5 Particle Size Analysis

Figure 73: Vermiculite Particle Size Distribution

Coming soon!

3 Acknowledgements

This work was supported by NASA Cooperative Agreement 80NSSC19M0214 to the Center for Lunar and Asteroid Surface Science (CLASS) as part of the Solar System Exploration Research Virtual Institute (SSERVI). The CLASS Exolith Lab gratefully acknowledges Kirk Scammon for collecting the XRF and XRD data. We also gratefully acknowledge Jesse Colangelo and Luis Zea who provided us with fused disk XRF data for basalt, funded by the University of Colorado, Boulder's Research Innovation Office. Simulant photos were taken by Matthew Villegas.

References

Gates-Rector, S. and T. Blanton (2019). The powder diffraction file: a quality materials characterization database. *Powder Diffraction 34*(4), 352–360.

Schofield, P. F., K. S. Knight, and I. C. Stretton (1996, 08). Thermal expansion of gypsum investigated by neutron powder diffraction. *American Mineralogist 81*(7-8), 847–851.

Vaughan, G., R. Brydson, and A. Brown (2012, jul). Characterisation of synthetic two-line ferrihydrite by electron energy loss spectroscopy. *Journal of Physics: Conference Series 371*, 012079.